Chapter - B

COMMINUTION & CLASSIFICATION

BOYUT KÜÇÜLTME & SINIFLANDIRMA

Outotec HIGmills; A Fine Grinding Technology

H. Lehto
Outotec Finland Oy

A. Paz
Outotec Pty Ltd, Perth, Australia

I. Roitto
Outotec Finland Oy

M. Åstholm
Outotec Sweden

ABSTRACT Global ore grades are declining while commodity demands continue to increase. Ore bodies requiring treatment are becoming increasingly complex requiring a finer grind size for maximum mineral recovery and grade. The demand for a finer grind size has set new challenges especially for grinding technology. Energy efficiency is a major driving force targeted for environmental sustainability and project viability. Fine grinding technology is utilized especially in concentrate regrinding to liberate the valuable minerals after the first stage of concentration. Maintaining the correct particle size and particle size distribution of the regrind product is crucial for downstream process performance.

Outotec HIGmills™ being based on existing, well proven stirred milling technology provide modern, sophisticated, flexible and energy efficient grinding solution for fine and ultra fine grinding. Outotec HIGmills™ offer the unique possibility for online control and optimization of regrind product particle size. This paper describes the basis of this online control possibility and how this fine grinding technology can be implemented in minerals processing especially in regrinding applications. The main focus of this paper is to describe the flexibility of this grinding solution to respond the fluctuations in feed rate tonnages as well as particle size fluctuations in concentrate regrinding.

1 INTRODUCTION

In 2012 Outotec launched a new fine grinding technology for the mineral processing industry. The technology has been utilised for more than 30 years in the calcium carbonate industry, its application, until recently, was unavailable for mineral processing. Further development backed by intensive test work has brought this technology to the minerals processing industry. Outotec is pleased to present a summary of this fine grinding technology.

Fine grinding technology use in the mineral process industry has increased over the last 10 years. This can be mainly attributed to processing finer grained mineral structures, which requires a finer grind for valuable mineral liberation. An example of an ore body with different mineral structure is given in figure 1. This ore body requires wide process adaptability and flexibility to cope with the life of mine ore variability.

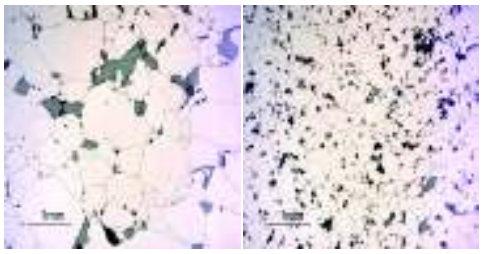

Figure 1. Mineral Structures

2 HIGMILL OPERATIONAL PRINCIPLES

In a typical application, the HIG process begins with the regrinding circuit feed being pumped to a scalping cyclone upstream of the mill which classifies the target size material off from the feed and defines the pulp density. The defined underflow is then mixed with water to optimal grinding density and pumped into the mill at base level. The slurry enters a grinding chamber containing grinding media (beads) and rotating discs which provide momentum to stir the charge against a series of stationary counter discs. The particles are ground by attrition between the beads.

As the flow transfers upwards, the ore slurry passes through the rotating discs and the free space between the static counter discs lining the wall (see Fig.2). Depending on the application there may be up to 30 sets of rotating and static discs. Due to the vertical arrangement of the mill, classification is conducted simultaneously throughout the grinding process with larger particles remaining longer at the peripheral, while smaller particles move upwards. The process is typically a single pass with no external classification necessary.

Gravity keeps the media compact during operation, ensuring high intensity inter-bead contact and efficient, even energy transfer throughout the volume. The disc configuration and the whole chamber geometry have been optimized for efficient energy transfer to the bead mass, internal circulation and classification.

With the grinding media evenly distributed, the ore particles remain in constant contact, significantly increasing grinding efficiency. The product discharges at atmosphere at the top of the mill. The combined cyclone overflow and mill discharge are the circuit product.

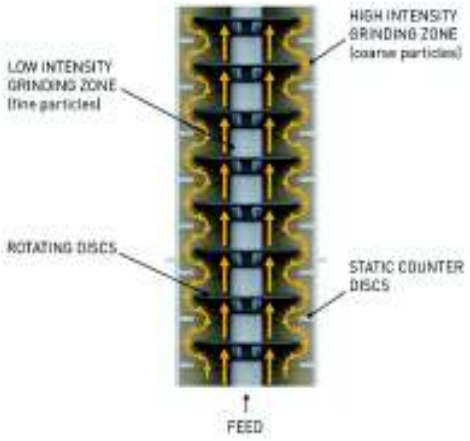

Figure 2. Optimal Grinding Conditions

2.1 HIGmill™ Control Philosophy

The flow from upstream processes can vary remarkably due to fluctuations in ore grade and quality. Also the target fineness can vary because of variations in the ore mineralogy.

HIGmill offers a unique opportunity to optimize product fineness on-line through the use of ACT (Advanced Control Tools) expert system. This is due to the HIGmill™ having a variable speed drive to control the impeller shaft speed, which in turn controls the power input into the material.

A set point for the specific grinding energy (SGE) is determined to achieve the product fineness. The ACT expert control system uses feed forward and feedback control principles.

The feed forward control principle is used by measuring scalping cyclone feed quantity which is measured by flow and density meters and adjusts the mill shaft speed to reach target energy per total feed flow. This principle ensures the target SGE is reached at all times even the throughput varies.

The feedback control principle is used by measuring the particle size distribution with

an on-line by Outotec PSI and adjusts the shaft speed to maintain a constant product size, (see fig. 5).

The make-up grinding beads are fed continuously to the mill along with the slurry feed. If there is a permanent large scale change in throughput or in PSD target level the bead charge is increased or decreased to the new optimal level to ensure that the online control with tip speed can be fully utilized.

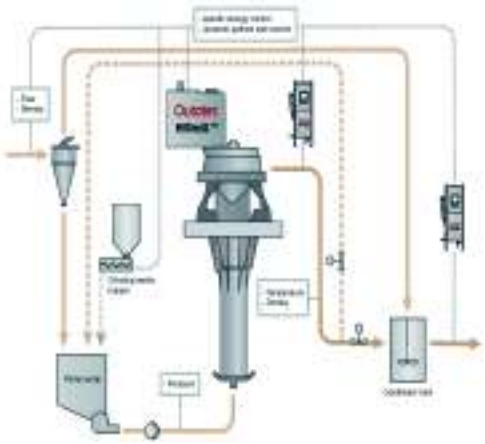

Figure 5. HIGmill Flowsheet

3 BENEFITS

3.1 Largest Units in Operation

Over 260 HIGmills have been put into service, with installed mill power up to 5,000 kW, making the HIGmill™ the largest fine grinding units in the market place to date. The Outotec HIGmill™ comes in various drum diameters. The Mill heights can be varied to optimize the media load and power input for specific applications. Chamber volumes range from 400 to 27,500 litres with corresponding drives from 132 to 5,000 kW (table 1). The HIGmill™ is the only ultrafine grinding technology in commercial use that can use small size high density grinding media in mill sizes above 3,000 kW.

Table 1. HIGmill™ Size Range

Type	HIG 132	HIG 300	HIG 500	HIG 700
Installed Power [kW]	132	300	500	700

Type	HIG 900	HIG 1100	HIG 1600	HIG 2300
Installed Power [kW]	900	1100	1'600	2'300

Type	HIG 3000	HIG 3500	HIG 4000	HIG 5000
Installed Power [kW]	3'000	3'500	4'000	5'000

3.2 Compact and Simple Installation

The benefit of high power intensity and vertical installation is a very small foot prints (see fig. 3). The head room over the mill is small and the flanged, split shell construction reduces the space needed for maintenance. The top supported, hanging arrangement keeps the floor and sides clear, simplifying maintenance and emptying the beads.

Gravity together with an internal hydroclassifier prevents the grinding media from escaping the mill by pushing the grinding beads back down into the milling process, and lets through only the fine ground slurry.

Figure 3. Typical HIGmill Installation - 3 x 5MW

3.2.1Maintenance Issues

The drum segments and wear components have been specifically designed to make maintenance simple and quick. The casing is flanged vertically so that it can be split down the centre into two halves that can be moved apart on a railing system. After exposing the internals, changing of discs and liner segments can be done individually by a team of two skilled mechanical trade personnel.

Wear of the discs is even around the circumference. The wear is faster in the bottom part of the mill and typically the lowest discs may have to be replaced before the total set is changed. For total set change, a spare shaft ready for installation is an option (see fig. 4). Wear components can be lined with polyurethane, metal hard facing or natural rubber depending on application. The critical components of the mill and gears can be delivered in short time. A large number of spares are available in stock for fast shipment and delivery.

Figure 4. Simple maintenance

3.3 Operational Flexibility

A wide range of grinding applications can be addressed as the HIGmill™ has an excellent flexibility to adapt to fluctuating process conditions. Typical applications for the HIGmill™ is the regrinding of concentrates (eg. magnetic, flotation), iron ore tertiary grinding, precious metal ores, and fine grinding for hydrometallurgical processes.

Both ceramic and steel beads can be used. Ceramic media is typically used for sulphide concentrate regrinding to prevent iron contamination on the sulphide mineral surface, which would otherwise result in poorer flotation recovery and grade.

The HIGmill™ can use a wide range of grinding media diameter which depends on the application: 0.5-1.5 mm in ultra fine, 1-3 mm in fine grinding and 3-6 mm in coarse grinding, where the grinding size is defined as follows:

- Coarse range, F80 100-300 µm, P80 50-100 µm
- Fine range, F80 50-100 µm, P80 20-60 µm
- Ultra fine range F80 <70 µm, P80 <20 µm

4 TEST WORK

4.1 Test Units

Outotec has two test unit sizes available for pilot test work. The test work produces a performance curve: particle size distribution versus specific grinding energy (SGE).

A semi-continuous test can be conducted in the HIG 7 unit (6 litre/7.5 kW) and is performed with a 50kg sample. The test sample is fed several times (steps) through the mill with one set of parameters and constant SGE which increases SGE in steps. Sampling is performed at each step.

A continuous test is conducted with the HIG 30 unit (18 litre/30 kW) and is performed with a 150kg to 250kg sample. The test sample is fed only once through the mill with multiple SGE points. The tip speed (m/s) is changed to deliver different SGE. Sampling is performed to represent each SGE point.

A continuous test can also be performed with HIG 7.5 unit with the same principles.

Minimum of a single parameter basic test is required for process sizing. In an optimal case, a larger sample is required so that more basic parameters can be tested. Test parameters are slurry milling density, retention time, tip speed, mill internal geometry, media charge, bead size/distribution and bead material. The measured test variables are power draw, feed rate, milling density solids and product particle size.

Typical process parameters for industrial operations are:

- Feed solids 30 % by volume (i.e. 50 % by weight if solids density 2,7)
- About 60 % of the mill volume is filled with beads
- Typical bead material is ceramics (i.e. zirconia-alumina-silicate, density 3.8-4.2 kg/dm³). Steel and high density (<6 kg/dm³) ceramics are options
- Bead size 0.5-6 mm depending to the F80 and P80
- Tip speed 4-8 m/s in smaller units, 8-12 m/s in larger units
- Typical Retention time 1-3 minutes
- Specific grinding energies from 5 up to 100 kWh/t
- Power intensity, kW/m³, is high 100-300 kW/m³

4.2 Test Results

Outotec has undertaken test work on a wide range of minerals and process variables which enabled Outotec to gain a better understand the process variables effect on process design.

A special feature of the HIGmill is that energy efficiency remains constant through a wide variety of operational parameter combinations; flow rates, tip speeds, and media filling rates. Figure 6 depicts three different flow rates with specific grinding energy (SGE) versus product fineness. Within each flow rate, each SGE point is generated by varying the shaft speed. The graph shows the product fineness is directly proportional to SGE input.

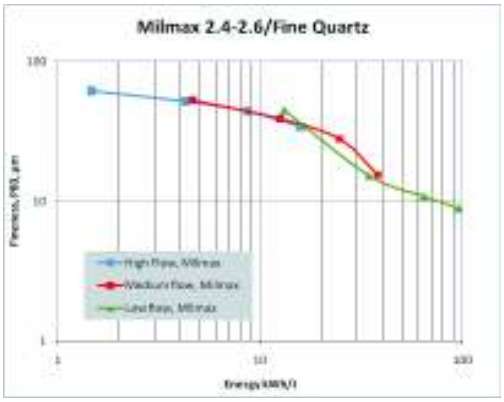

Figure 6. Consistent energy efficiency

Power draw increases exponentially if the tip speed is increased (see fig. 7). If the shaft speed is doubled the power draw is tripled. This makes it possible to control PSD on-line and dampen flow rate and quality fluctuations. The PSD set point can be changed on line by changing tip speed.

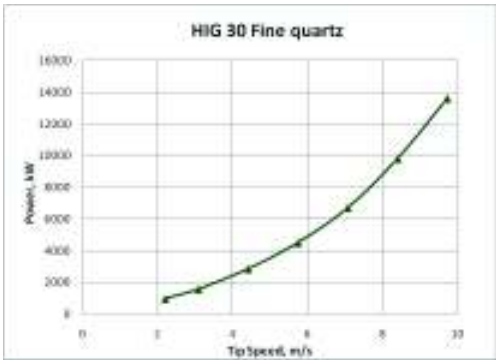

Figure 7. Power draw vs. Tip speed

The same energy efficiency is achieved with different grinding media filling volumes (see fig. 8). This makes it possible to control the PSD on-line and to account for filling volumes or bead wear. The power input and PSD can be changed on line by changing tip speed.

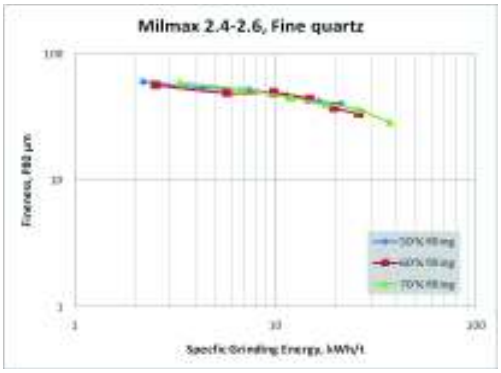

Figure 8. Media filling volume

In figure 9, it can be seen that there is almost linear correlation between media filling rate and power draw. Thus, media charge increase is directly related to power draw increase. The power draw is directly related to SGE (kWh/t). If there is a 10% v/v decrease in media charge from 70%v/v to 60%v/v, the result is a ~20% decrease in SGE. Therefore to obtain the same SGE and grind size; the feed rate must also decrease by ~20%.

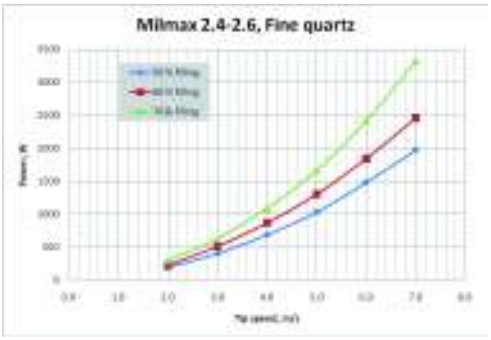

Figure 9. Media filling control strategy

Semi-Continuous and continuous test work has given similar results (see fig. 10). These results give a reliable scale-up from semi continuous (HIG 7) to continuous (HIG 30). As per other fine grinding technology we expect the HIGmill^{TM} to scale directly up to the industrial size.

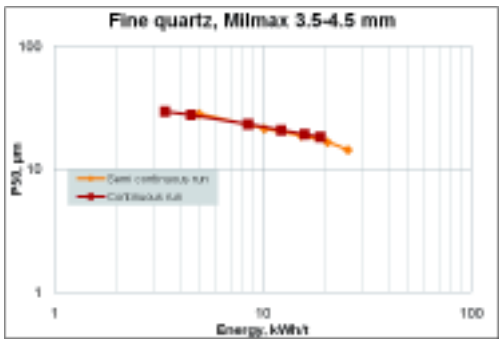

Figure 10. Reliable Scale-up

Comparison test work was conducted with a tertiary / regrind ball mill in the magnetite application. The HIGmill^{TM} minimised energy usage by up to 40 to 50% compared to the process benchmark, (see fig 11). We can clearly see that the Energy efficiency in HIGmill^{TM} is significantly better compared to process benchmark values, the difference being up to 5 kWh/t (~50 %).

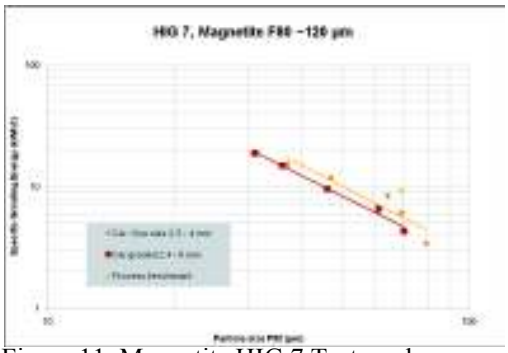

Figure 11. Magnetite HIG 7 Test work

5 SUMMARY

The HIGmill^{TM} is an innovative and unique grinding tool provides advanced, energy efficient fine and ultra-fine grinding for new projects or can deliver value-adding, optimisation solutions for existing installations. The HIGmill^{TM} is supplied with a variable speed drive which enables an effective control strategy for controlling the product fineness.

Fragmentation Modelling and the Effects of ROM Fragmentation on Comminution Circuits

S. Esen
Mining Services, Orica Australia Pty Ltd, Australia

ABSTRACT This paper reviews the blast fragmentation models developed to date and discusses the effects of the run-of-mine (ROM) fragmentation on the comminution circuits. The fragmentation model developed by the author is presented in detail. Its use in numerous mine-to-mill projects is briefly discussed. The fragmentation modelling framework is based on the combination of Kuz-Ram model to model the coarse end and an engineering approach to model the fines. It is well-known that the Kuz-Ram model underestimates the fines generated by blasting. The model is further validated by new data sets (actual sieving data). It is shown that the model is rather robust in estimating the fines generated by blasting. The mine-to-mill studies have shown that -10mm size generated by blasting can be considered a key performance index as this fraction has a significant effect on mill throughput. The mine sites have increased their powder factors significantly which resulted in mill throughput increases of 5 to 30%. Two case studies were presented as examples of the use of the fragmentation model in mine-to-mill projects. Some of the opportunities to further reduce the energy consumed by mining processes are also highlighted.

1 INTRODUCTION

Traditionally the mining industry manages the units of operations (drill&blast, load&haul, crushing and grinding) separately by adopting extreme control measures in operational and capital expenditure. Costs are generally managed separately for mining and milling cost centres. Cost minimisation is achieved through focussing on achieving production targets at minimum cost. This approach does not necessarily result in the reduction of the total mine operating cost (mining and milling). Investigations by several researchers to date have shown that all the processes in the mine to mill value chain are inter-dependent and the results of the upstream mining processes (especially blast results such as fragmentation, muckpile shape and movement, rock damage) have a significant impact on the efficiency of downstream milling processes such as crushing and grinding (Eloranta 1995, McKee et al. 1995, Kojovic et al. 1998, Kanchibotla et al. 1998, Simkus and Dance 1998, Scott et al. 1999, Kanchibotla et al. 1999, Valery et al. 1999, Valery et al. 2004, Dance et al. 2006, Esen et al. 2007, Valery et al. 2007, Kanchibotla and Valery, 2010).

Numerous mine-to-mill projects to date resulted in mill throughput increases of between 5 and 30% depending on the ore strength and communition properties. Fragmentation is the most significant component of the mine-to-mill value chain. It was shown that the effect of finer fragmentation on mill throughput is more significant than changing the operational parameters of the grinding circuit (Dance et al. 2006, Esen et al. 2007).

Drill and blast is understood to be the most energy efficient and cheapest way of reducing particle size compared to downstream operations, as shown in Table 1. The use of greater energy input in the blasting unit operation is less costly than expending the energy downstream.

Table 1. Energy and cost calculations by unit operations at a hard rock gold mine (Esen, 2010)

	Specific energy kwh/t	Energy factor	Cost factor
Drill and Blast	0.1 – 0.25	1	1
Load and haul	0.2 – 0.5	1 - 5	2 - 10
Crushing	1 – 2	4 -20	2 - 10
Grinding	10 – 20	40 - 200	8 - 20

Fragmentation can also have a notable impact on the economics of recovery in heap leaching as demonstrated by Sheikh and Chung (1987), in a study conducted at the Denison mine (Ontario, Canada). They concluded that the viability of heap leaching processing in this operation depended upon the alternative of maintaining stockpiles of broken ore for long periods of time, or adopting blast fragmentation optimisation strategies through the implementation of appropriate blast designs.

This paper discusses the fragmentation modelling which is used in carrying out the mine-to-mill simulations, the effect of feed size on crusher and SAG mill, and the application of the author's fragmentation model in mine-to-mill projects with two case studies.

2 BLAST FRAGMENTATION MODELLING

2.1 Background

The need to provide engineering solutions to full scale blasting problems such as those involving the optimisation of Run-of-Mine (ROM) fragmentation, has driven the development of several fragmentation models. These include empirical as well as advanced numerical techniques. Appendix 1 gives a chronological summary of the developments in applied fragmentation modelling over several decades.

The most commonly used empirical models are those based on the determination of parameters to fit functions that can adequately describe the expected distribution of rock fragments for a given set of conditions. In these approaches, the most widely applied fragmentation distribution function has been the Rosin-Rammler distribution or simplified versions of the same (Rosin and Rammler 1933, Kuznetsov 1973, Cunningham 1983, Yalun 1987, Rollins and Wang 1990, Aler et al. 1996). The Rosin-Rammler function has been recently replaced by the Swebrec function (Ouchterlony 2003,2005). This is a more refined representation of the size distribution of fragmented rock materials.

Swebrec function contains three parameters, x_{50}, x_{max} (mean and maximum fragment size, respectively) and an undulation parameter b. It has been shown that this function can describe the sieved data with a coefficient of determination R^2 better than 0,995 in 95% of the fragmentation data encountered (Ouchterlony 2003,2005). This function has been tested against hundreds of sieved size distributions from bench blasts in quarries, reef blasting, model blasting and crushing.

The Swebrec function is as follows:

$$P(x) = 1/\{1+[\ln(x_{max}/x)/\ln x_{max}/x_{50})]^b\} \quad (1)$$

In the late 1990s, developments in fragmentation modelling saw the introduction of the two component modelling approach which mainly allowed for improvements in the prediction of fine fragmentation (Kanchibotla et al. 1999, Djordjevic 1999, Thornton et al. 2001). Subsequently Onederra and Esen (2004) developed a more accurate way of estimating the potential volume of crushed material resulting from the crushing and shearing stages of blasting.

Above fragmentation models have been successfully used in numerous projects to date. There are also significant advances made with the numerical models (Minchinton and Lynch 1996, Ruest et al. 2006, Dare-Bryan et al. 2010); however, their use is not widespread and only used at a high-level research/consulting projects. This paper doesn't attempt to review these models as it is not within the scope of this paper.

2.2 Onederra and Esen's (2004) fragmentation model

Fines (usually -10mm term) in blasting is considered as one of the most important KPIs in the mine-to-mill concept. Mine-to-mill projects to date showed us that operations that require higher mill throughputs should maximize a maximum amount of fines (-10mm fraction). These projects required an accurate estimation of fines and complete ROM fragmentation size distributions.

The Kuz-Ram model's poor ability to describe the fines was one of the major reasons why the Two Component Model (Djordjevic 1999), the Crush Zone Model (Kanchibotla et al. 1999) and Onederra and Esen's (2004) model were developed at the JKMRC. All combine two Rosin-Rammler distributions or components, one for the coarse part of the curve and one for the fines. Onederra and Esen (2004) showed that the Kuz-Ram model is not able to satisfactorily predict the complete size distribution of fragments, particularly in the fine and intermediate size fractions (Figure 1). The need to be able to predict the amount of fines from blasting has driven the development of a new engineering model.

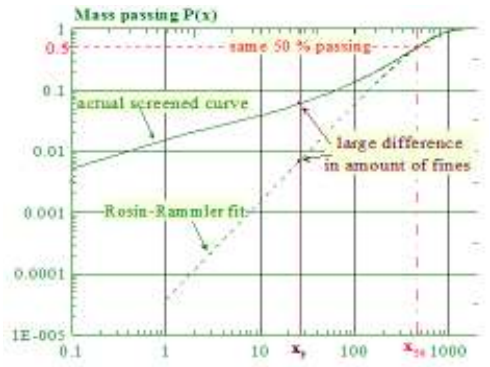

Figure 1. Kuz-Ram's limitation in predicting the fines and intermediate regions

Onederra and Esen's (2004) model is detailed in their paper. Their framework is based on the combination of a new model to predict the radius of crushing around a blasthole with a model to predict the volume of crushed material resulting from major radial cracks (Figure 2). Other sources of fines including liberation of infilling from discontinuities, particle collisions and post-blast processes are excluded to simplify the modelling process. Based on the analysis of a number of full scale blasting surveys, their study has confirmed that upon detonation of an explosive, the region of crushing around a blasthole is not the only source of fines. However, the proportion of fines generated by the crushed zone in low strength rocks is relatively greater than in medium to high strength rock types, and therefore should not be neglected.

Validation results based on seven case studies have shown that there is good agreement between model predictions and the measured proportion of fines, at the assumed cut off point of 1mm.

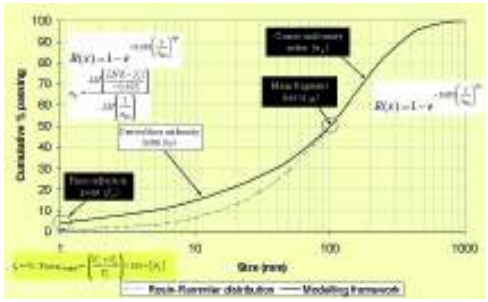

Figure 2. Onederra and Esen's model

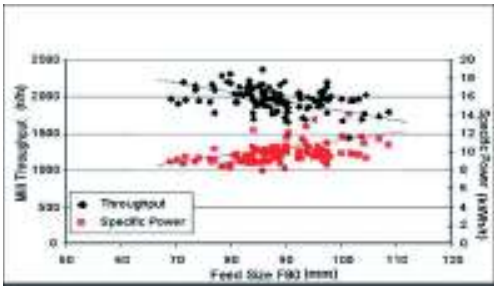

Figure 3. SAG feed size versus throughput & specific energy at a copper operation (Dance et al. 2006)

3 FEED SIZE EFFECT ON CRUSHERS AND SAG MILLS

Primary crushers are sensitive to oversize rocks because they cause hang-ups and also increase the power draw. It is generally accepted that the primary crushers reduce only the top size of run of mine and most of the fines (- 10mm) are generated through blasting. The Key performance Index (KPI) is the Closed Side Setting (CSS) of the primary crusher. If the ROM fragmentation is finer, then there is a scope to minimize the CSS to deliver finer SAG feed.

It is important to highlight that any mine-to-mill optimization work focuses on feed size to the SAG Mills (Dance et al. 2006). SAG mills require a certain ore feed size distribution to operate efficiently. This feed is supplied to the mill by the Primary Crusher, which is also influenced by the size distribution achieved from blasting. Significant effort has been spent at a number of operations to relate SAG mill throughput with SAG mill feed size. Very good correlations have been obtained demonstrating that the finer the topsize and F80 of the mill feed, the higher the mill throughput. Figure 3 shows correlations between SAG mill feed size as measured by on-line image analysis systems and SAG mill throughput and specific energy consumption (kWh/t) at a copper ore operation (Dance et al. 2006).

The ideal size distributions, which result in maximum mill throughput and performance, will depend on the breakage characteristics of the ore (rock strength) as well as the operating conditions of the mill (lifter design, grate design, mill speed and rock charge). In general terms, higher throughput for these harder domains may be achieved when the SAG mill feed has (Dance et al. 2006):

- as fine a top size as possible;
- the smallest possible amount of 25 to 75mm intermediate size material and
- a maximum amount of –10 mm fines.

Figure 4 gives a general indication of the strategy required to achieve an ideal SAG mill feed size distribution. The SAG mill feed topsize is mostly controlled by the Primary Crusher. The intermediate size material which is usually in the size range between 25 to 75mm (this range will vary according to ore hardness) is reduced both by appropriate fragmentation in the mine and optimal operation of the Primary Crusher. Fines (-10mm material) are largely generated by blasting. Depending on ore hardness, some fines can be also generated by inter-particle breakage in the crusher, especially when it is choke fed. The more fines in the feed, the higher the SAG mill throughput: a relatively simple relationship.

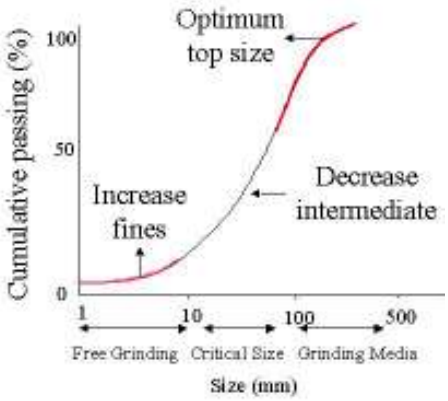

Figure 4. SAG mill feed size distribution (Dance et al. 2006)

4 UPDATE WITH THE FRAGMENTATION MODEL AND ADDITIONAL VALIDATION DATA

Given the success of Swebrec function in fitting the fragmentation data, it was decided to use the modelling results (x_{50},x_{70}, x_{80} and % passing at 1mm data) and force Swebrec function to pass through these four data sets using below simplified Swebrec function:

$$P(x) = \frac{1}{1 + \left[\frac{\ln(x_{max}/x)}{\ln(x_{max}/x_{50})}\right]^{a}} \quad (2)$$

where xmax and a are fitting parameters.

Figures 5 to 8 show the application of this approach to four cases in which fragmentation data is partially or fully sieved. It is shown that the updated model compares well with the experimental data.

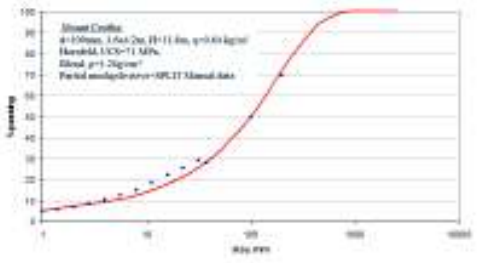

Figure 5. Mount Cootha Quarry fragmentation data – experimental vs model fit

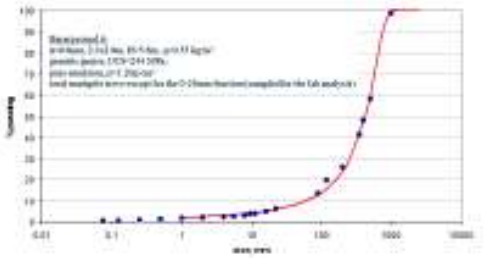

Figure 6. Bararp Quarry fragmentation data – experimental vs model fit

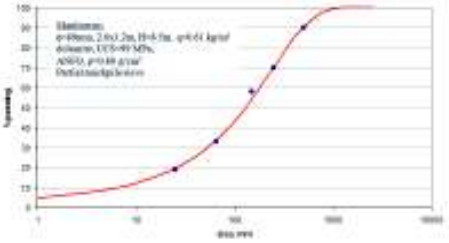

Figure 7. Manitowoc Quarry fragmentation data – experimental vs model fit

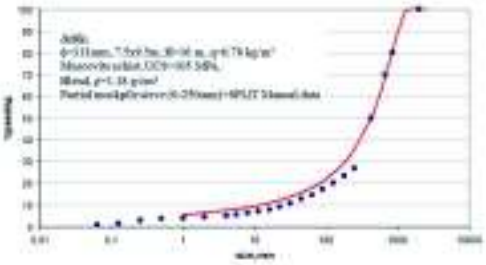

Figure 8. Aitik copper/gold fragmentation data – experimental vs model fit

Some sieve data were collected from a large open pit gold mine in Australia. The sieve sizes were 10mm and 30mm. Image analysis was also conducted to determine the size distribution of the blasted muckpile. Figure 9 shows the comparison of the sieve data versus fragmentation model. It is shown that the results compare well at 10 and 30mm sizes where the sieve data is available (Esen, 2010).

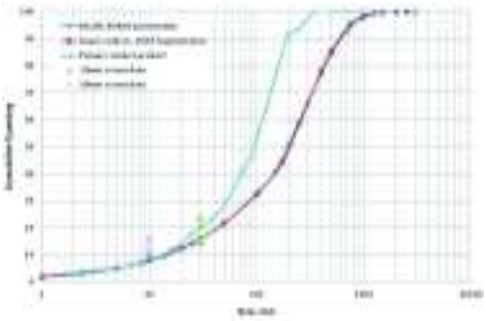

Figure 9. Comparison of the sieve data at 10 and 30mm with the model

5 THE APPLICATION OF THE FRAGMENTATION MODEL IN MINE-TO-MILL PROJECTS

The fragmentation developed by the author has been used in numerous mine-to-mill projects globally. Two of the case studies are discussed in detail to demonstrate the application of the model.

The first case study is from a large copper-zinc operation in South America. This operation wanted to increase the throughput of a particular ore type that historically processed between 2,300 and 3,300tph. The study revealed a number of opportunities for improving ROM fragmentation through blast design changes (Table 2).

Table 2. Baseline and modified blast design parameters at a large copper-zinc operation in South America (Esen et al. 2007)

Design	Hole Dia (mm)	Burden x Spacing (m)	Powder Factor (kg/m^3)	Predicted % -25mm	Predicted P80 (mm)
Current	311	7 x 8	1.15	30.7	401
Modified	311	6 x 7.5	1.62	44.4	175

A trial blast was conducted on material containing this ore type and resulted in significantly finer fragmentation. Figure 10 shows a trend of SAG mill tonnage over time before, during and after this modified blast material was processed. For the entire period shown, the ore type was the same and was mined from a similar area of the pit. The values in Figure 7 show the mill tonnage increased from 3,500 to 4,000tph before to around 5,000tph for the modified blast material. With the stockpile depleted and normally blasted material sent to the concentrator, tonnage returned to below 4,000tph. The increase in mill throughput was 25 to 40%, exceeding all expectations and more than compensated for the 8¢/tonne higher blasting costs. The mine-to-mill trials conducted after this work included pebble crusher, grate open area, SAG mill ball charge, a slight change in the blast pattern. This helped the mine consistently achieve SAG mill throughputs above 4000tph for this specific ore type.

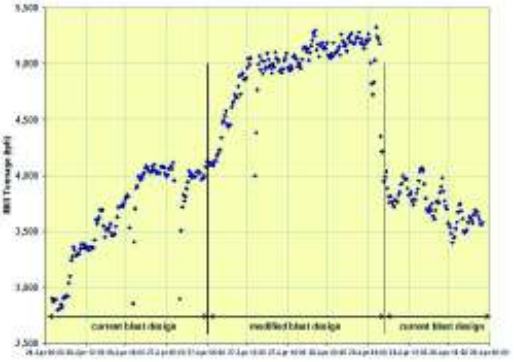

Figure 10. Trend of concentrator tonnage during modified blast trial (Dance et al., 2007)

Another case study was from a gold mine in Ghana. The mine-to-mill project was conducted on November/December 2010 period. This mine used to operate at a powder factor of 1.20kg/m^3 (Table 3) and having a SAG mill F80 of 40mm. An alternative blast design (Table 3) was suggested at a powder factor of 1.40kg/m^3 with some other design changes. The mill F80 decreased to 30mm as shown in Figure 11 and the mill throughput increased by 23% (from 475tph to 587tph) with the alternative blast design (Esen and Crosby, 2011).

Table 3. Blast design parameters for the base case and modified blasts at a gold mine in Ghana

	Baseline	Alternative blast design
Hole diameter, mm	165	165
Bench height, m	9	9
Powder factor, kg/m^3	1.2	1.4
F80, mm	284	251
% -10mm	20.4	22.6

Figure 11. Mill feed F80 data for SAG1 and SAG2 Mills

6 CONCLUSIONS

This paper reviewed the existing empirical fragmentation models including the author's model which is currently updated using Swebrec function. The model was validated with four case studies. The updated model appears to compare well with the measured data sets.

The fragmentation model was used in numerous mine-to-mill projects in which mill throughput increased between 5 and 30%. In these projects, -10mm fraction that is generated by blasting appear to be the most important KPIs in any mine-to-mill project.

Two case studies were presented to demonstrate the benefits of the mine-to-mill. The first case study was from a large copper-zinc operation. This operation increased their throuhput with the modified blast by 25-40% exceeding all expectations.

Another case study was from a gold mine in Ghana. The optimised blast design resulted in the reduction of the mill feed (mill F80 decreased from 40mm to 30) and increased the mill throughput by 23% (from 475tph to 587tph).

The threat of global warming, increased cost of energy, limited availability of water resources and social and legislative pressures are creating a need in the mining industry to reduce energy and water consumption. Many mining companies are now routinely accounting for the energy and water consumed and greenhouse gases produced per unit of final product and are making special efforts to operate in a more sustainable manner.

Recent reviews to date have shown the value of the use of the high-intensity blasting, HPGRs in comminution circuits and pre-concentration in future mining circuits.

REFERENCES

Aler, J, Du Mouza, J and Arnould, M, 1996. Measurement of the fragmentation efficiency of rock mass blasting and its mining applications. Int. J. Rock Mech. Min. Sci., 33, No2: 125-139

Cunningham, C V B, 1983. The Kuz-Ram model for prediction of fragmentation from blasting. Proceedings of the first international symposium on rock fragmentation by blasting, Lulea, Sweden, 439-453.

Cunningham, C V B, 1987. Fragmentation estimations and the Kuz-Ram model - Four years on. Proceedings of the second international symposium on rock fragmentation by blasting, Keystone, Colorado, 475-487.

Cunningham, C.V.B. 2005. The Kuz-Ram fragmentation model—20 years on. In R. Holmberg (ed.), Proc. 3rd EFEE World Conf. on Explosives and Blasting, Brighton, UK, 13–16 September, pp. 201–210. Reading, UK: European Federation of Explosives Engineers.

Dance, A., Valery Jnr., W., Jankovic, A., La Rosa, D., Esen, S., 2006. Higher Productivity Through

Cooperative Effort: A Method Of Revealing And Correcting Hidden Operating Inefficiencies. SAG2006 – HPGR, Geometallurgy, Testing. International Conference on Autogenous and Semiautogenous Grinding Technology, Volume 4, 375 – 390, Vancouver, Canada.

Djordjevic, N, 1999. Two-component of blast fragmentation. Proceedings of 6th international symposium of rock fragmentation by blasting - FRAGBLAST 6, Johannesburg, South Africa. South African Institute of Mining and Metallurgy, 213-219.

Eloranta, J. 1995. Selection of powder factor in large diameter blastholes, EXPLO 95 Conference, AusIMM, Brisbane, September, PP 25-28.

Esen, S., LaRosa, D., Dance, A., Valery, W., Jankovic, A., 2007. Integration and optimisation of Blasting and Comminution Processes. EXPLO 2007. Australia. pp 95-103.

Esen, S. 2010. Mine to Mill Process Integration and Optimisation. Unpublished presentation.

Esen S., Crosbie, R. 2011. Integration and Optimisation of Blasting and Crushing Practices at AngloGold Ashanti – Iduapriem. Final Report. Metso Minerals.

Hjelmberg, H, 1983. Some ideas on how to improve calculations of the fragment size distribution in bench blasting. Proceedings of the 1st international symposium on rock fragmentation by blasting, Lulea, Sweden, 469-494.

Jankovic, A, Valery W, Dikmen S, Esen, S, Sader P. 2010. Process Integration and Optimisation from Mine to Mill for Newmont Boddington Gold Mine. Progress Report, Metso Minerals.

Kanchibotla S. S., Morrell S., Valery W., and O'Loughlin P., 1998. Exploring the effect of blast design on SAG mill throughput at KCGM, Proc. Mine-mill conf., Brisbane, 1998.

Kanchibotla S.S., Valery W., and Morrell S. 1999. Modelling fines in blast fragmentation and its impact on crushing and grinding, Explo-99, Kalgoorlie.

Kanchibotla S.S., Valery W. 2010. Mine-to-mill process integration and optimization – benefits and challenges. 36th Annual Conference on Explosives and Blasting Technique, International Society of Explosives Engineers, Orlando, USA.

Kojovic T., Kanchibotla S. S., Poetschka N.L., and Chapman J. 1998. The effect of blast design on the lump:fines ratio at Marandoo iron ore operations, Proc. Mine-to-mill conf., Brisbane, 1998.

Kuznetsov, V M, 1973. The mean diameter of fragments formed by blasting rock. Soviet Mining Science, 9: 144-148.

Just, G D and Henderson, D S, 1971. Model studies of fragmentation by explosives. Proc. 1st Aust.-New Zealand Conf. Geomech., Melbourne, 1: 238-245.

Larsson, B, Hemgren, W and Brohn, C E, 1973. Styckefallsutredning. Skanska, Cementgjuteriet. (original not seen).

Larsson, B, 1974. Fragmentation in production blasting. Proc. of Bergsprangingskommite, Stockholm (original not seen).

Lilly, P A, 1986. An empirical method of assessing rock mass blastability. Proceedings of the AUSIMM-IE Aust. Newman Combined group, large open pit mining conference, 89-92.

McKee, D J, Chitombo, G P and Morrell, S, 1995. The Relationship Between Fragmentation in Mining and Comminution Circuit Throughput. Minerals Engineering, 8: 1266-1274.

Minchinton, A. and Lynch, P.M., 1996, "Fragmentation and Heave Modelling Using a Coupled Discrete Element Gas Code", Proceedings Fifth International Symposium on Fragmentation by Blasting, Montreal, Canada, 25-29 Aug, A.A. Balkema, Rotterdam, pp. 71-80.

Rollins, R and Wang, S-W, 1990. Fragmentation prediction in bench blasting. Proceedings of the third international symposium on rock fragmentation by blasting, The Australasian Institute of Mining and Metallurgy, Brisbane, Australia, 195-198.

Rosin, R and Rammler, E, 1933. Laws governing fineness of powdered coal. J. Inst. Fuels, 7: 29-36.

Ruest, M., Cundall, P., Guest, A. & Chitombo, G. 2006. Developments using the particle flow code to simulate rock fragmentation by condensed phase explosives. Proceedings of the 8th International Symposium on Rock Fragmentation by Blasting (Fragblast 8), Santiago, Chile, 7-11 May. Santiago: Editec, pp. 140-151.

Rustan, A, Vutukuri, V S and Naarttijarvi, T, 1983. The influence from specific charge, geometric scale and physical properties of homogeneous rock on fragmentation. Proceedings of the 1st international symposium on rock fragmentation by blasting, Lulea, Sweden, 115-142.

Onederra, I, Esen, S and Jankovic, A, 2004. Estimation of fines generated by blasting - applications for the mining and quarrying industries. IMM transactions, Vol 113, No.4:237-247.

Ouchterlony, F. 2003. 'Bend it like Beckham' or a widerange yet simple fragment size distribution for blasted and crushed rock. EU project GRD-2000-25224. Less Fines project int. techn. rpt no. 78. Leoben, Austria: Montanuniversitat.

Ouchterlony, F. 2005. The Swebrec function: linking fragmentation by blasting and crushing. Mining Techn. (Trans. of the Inst. of Mining & Met. A) 114:A29–A44.

Scott, A., Kanchibotla S.S., and Morrell S. 1999. Blasting for Mine to Mill Optimisation, Explo-99, Kalgoorlie.

Scott, A, David, D, Alvarez, O and Veloso, L, 1998. Managing fines generation in the blasting and crushing operations at Cerro Colorado Mine. Mine to Mill 1998 Conference. The Australasian Institute of Mining and Metallurgy, Brisbane, Australia, 141-148.

Scott, A., Michaux, S. P. and Onederra, I. A. 2009. Characterising dust generation from blasting.. In: Sanchidrian, J. A.,Fragblast 9 - 9th International Symposium on Rock Fragmentation by Blasting. Fragblast 9, Granada, Spain,(663-671). 13-17 September, 2009.

Sheikh, A M and Chung, S H, 1987. Predicting fragmentation sizing profiles for different blasting patterns. Second international symposium on rock fragmentation by blasting, Keystone, Colorado.

Simkus R., and Dance A. 1998. Tracking hardness and size : Measuring and monitoring ROM ore properties at Highland valley copper, Proc. Mine to Mill Conf., Brisbane. Fourney W L and Dick R D (Ed.), 521-530.

Stagg, M S, Rholl, S A, Otterness, R E and Smith, N S, 1990. Influence of shot design parameters on fragmentation. Proceedings of the third international symposium on rock fragmentation by blasting, The Australasian Institute of Mining and Metallurgy, Brisbane, Australia, 311-317.

Thornton D, Kanchibotla S. and Brunton I. 2001. Modelling the Impact of Rockmass and Blast Design Variation on Blast Fragmentation. Proceedings of EXPLO 2001, Hunter Valley, NSW, Australia, October 2001. The Australian Institute of Mining and Metallurgy, 331-345.

Valery Jnr., W., Kojovic, T., Tapia-Vergara, F. and Morrell, S. 1999. Optimisation of blasting and sag mill feed size by application of online size analysis. IRR Crushing and Grinding Conference, Perth, WA 29-31 March.

Valery Jnr., W., La Rosa, D., Jankovic, A. 2004. Mining and Milling Process Integration and Optimisation, presented at the SME 2004 Conference, Denver, CO. 23-25 February 2004.

Valery, W., Jankovic, A., La Rosa, D., Dance, A., Esen, S. and Colacioppo, J. 2007. Process integration and optimisation from mine-to-mill. Proceedings of the International Seminar on Mineral Processing Technology, pp. India. 577-581.

Yalun, 1987. A size distribution study of the blasted ore fragments in Shui-Chang open pit China. Second International symposium on rock fragmentation by blasting, Colorado, USA, 672-676.

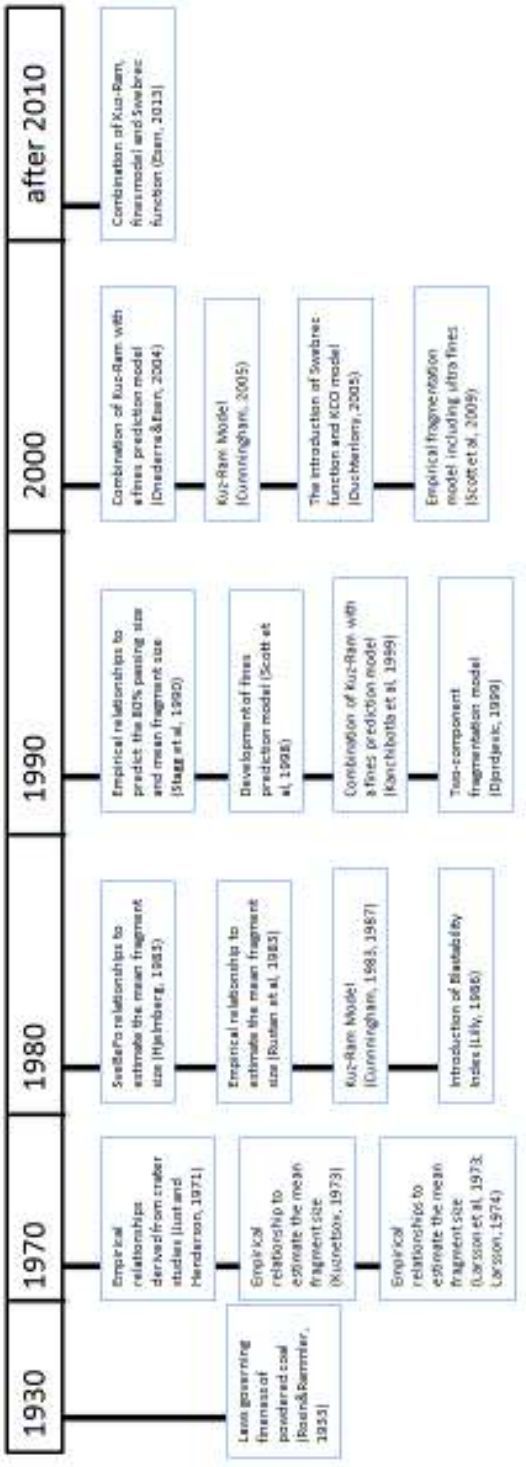

Appendix 1. Development of empirical blast fragmentation models.

Yapay Vollastonit ($CaSiO_3$) Üretiminin Mekanik Aktivasyonu

Mechanical Activation of Synthetic Wollastonite ($CaSiO_3$) Production

M. Göktaş
Bilecik Şeyh Edebali Üniversitesi, Bozüyük Meslek Yüksek Okulu, Doğal Yapı Taşları Bölümü, Bozüyük/Bilecik
M. Şener, M. Erdemoğlu
İnönü Üniversitesi, Mühendislik Fakültesi, Maden Mühendisliği Bölümü, Malatya

ÖZET Bu çalışmada, mermer işleme fabrikalarında ortaya çıkan mermer atık tozunun bir seramik hammaddesi olan yapay vollastonit ($CaO.SiO_2$ ya da $CaSiO_3$) üretmek üzere değerlendirilmesi araştırılmıştır. Bu amaçla, mermer atık tozuyla kuvars kumunun birlikte aşırı şartlarda öğütülmesinin vollastonit üretimi üzerine etkisi incelenmiştir. Bilyalı jet değirmeni yardımıyla çeşitli sürelerde kuru öğütme işlemleri yapılmış ve öğütülmüş karışım malzemeleri $CaSiO_3$ oluşturmak üzere tepkimesi amacıyla 900°, 1000°, 1100° ve 1200°C sıcaklıklarda çeşitli sürelerde kavrulmuştur.

Başlıca X-ışınları difraktometri yöntemi kullanılarak öğütülmemiş ve öğütülmüş tüm hammadde ve ürünlerin mineralojik karakterizasyonuyla birlikte SEM analizleri yapılmıştır. Sonuçlar, mermer atık tozu – kuvars tozu karışımının birlikte ve aşırı koşullarda öğütülmesi işleminin, vollastonit oluşum sıcaklığını düşürmek üzere bir mekanik aktivasyona yol açtığını göstermiştir.

Anahtar Kelimeler: Mermer atık tozu, yapay vollastonit, aşırı öğütme, mekanik aktivasyon

ABSTRACT In this study, production of synthetic wollastonite ($CaO.SiO_2$ or $CaSiO_3$), one of the raw materials of ceramics, was investigated to evaluate the marble waste dusts in marble processing plants. For his purpose, effect of milling of marble waste dusts together with quartz sand under intensive conditions on the production of wollastonite was studied. Dry milling was performed for various periods using jet ball mill, and milled mixture materials were roasted at temperatures of 900°, 1000°, 1100° and 1200°C to react to form $CaSiO_3$.

Mainly using the X-ray diffraction method, mineralogical characterisation of all raw materials and products, either unmilled or milled, were carried out along with SEM analysis. The results showed that milling of marble waste dust-quartz sand mixture together and under intensive conditions gives rise to a mechanical activation so as to decrease the wollastonite formation temperature.

Keywords: Waste marble dust, synthetic wollastonite, intensive milling, mechanical activation

1 GİRİŞ

1.1 Vollastonit

Son on beş yılda endüstriyel mineral pazarında önemli bir yeri olan vollastonit ($CaO.SiO_2$ ya da $CaSiO_3$), yaygın kullanım alanı ve bazı kendine özgü özellikleri nedeniyle önümüzdeki yıllarda da önemini koruyacak, başta seramik sanayi olmak üzere boya, plastik, kaplama, cam endüstrisi gibi pek çok alanda önemli bir hammadde olmaya devam edecektir. Endüstriyel bir mineral olan vollastonit, doğal kalsiyum metasilikat olarak tanımlanır (Andrews, 1970). Araştırmalarda kaydedilen hızlı ilerleme, bu mineral için pek çok endüstriyel kullanım alanı ve geleneksel minerallerin yerine kullanıldığında, vollastonitin pek çok avantaja sahip olduğunu kanıtlamıştır. İmalat esnasında karışım içindeki vollastonitin birleştirici rolü özellikle seramik endüstrisinde geniş uygulama alanları yaratmıştır. Vollastonit ile ilgili bir diğer önemli konu, sentetik olarak da üretilebilmesidir (DPT, 2001). Yapay vollastonit üretiminde mekanik aktivasyonun etkilerinin araştırıldığı bu çalışma, vollastonitin daha düşük maliyetle üretimi araştırmalarına katkı sağlanmış olunacaktır.

1.2 Mekanik Aktivasyon

Mekanokimya, kimyasal, fiziksel ya da fizikokimyasal durum değişiklerinin mekanik enerji aktarımının yoğun olduğu bir sistemde gerçekleşmesidir (Baláž, 2000). Mekanokimyasal bir ön işlem olan mekanik aktivasyon ise, kavurma ya da liçing gibi temel bir metalurjik süreç öncesinde mineralin bu süreçlerdeki reaktifliğini artırmak üzere uygulanır ve mekanik enerjinin yoğun biçimde aktarılabildiği öğütme değirmenlerinde gerçekleştirilir (Baláž, 2000; Wang ve Forssberg, 2007). Mekanik aktivasyonun başlıca etkisi, fizikokimyasal özelliklerinde değişikliğe yol açacak şekilde mineral tanelerinin ufalanmasıdır. Mekanik aktivasyon sırasında mineralin kristal yapısı bozulur ve daha reaktif türler oluşur. Böylece, aşırı şartlar altında öğütülmüş mineral, elden geçirileceği metalurjik süreç sırasında artık daha aktif olarak davranacak ve bu durum sürecin hızını artıracaktır (Baláž ve Achimovičová, 2006).

1.3 Yapay Vollastonit Üretiminin Mekanik Aktivasyonu

Kireçtaşından kireç elde edilmesi gibi mermer tozu ve kuvars tozunun kalsinasyonu sonucunda yapay kalsiyum silikat elde edilmektedir. Hem endüstriyel minerallerin mekanik aktivasyonu, hem de mermer toz atıklarından seramik sanayinde kullanılacak yapay kalsiyum silikat üretimi araştırmaları yapılmak üzere, çalışmada mermer toz atıkları ve kuvars tozu örnek mineral olarak seçilmiştir. Böylece, aşırı öğütme ile mekanik aktivasyona uğrayan mermer toz atıkları ve kuvars tozu karışımlarının yapılarındaki değişiklikler incelenmiş ve daha düşük kavurma sıcaklıklarında vollastonit elde edilebilmiştir.

2 MATERYAL VE YÖNTEM

Çalışmada; mermer fabrikalarından kesme ve parlatma işlemleri sırasında ortaya çıkan atık sularını arıtan ve mermer tozlarının seramik sanayinde kullanılmak üzere; yapay vollastonit üretiminde kullanılabilme imkanının araştırılması için mümkün olduğunca beyaz mermer işleyen fabrikaların bulunduğu yerlerden numuneler alınmıştır.

Öğütme işleminin yapay vollastonit üretiminde mekanik aktivasyona ne derecede katkı sağladığını gözlemlemek için, öğütülmemiş ve öğütülmüş tüm hammadde ve ürünlerinin mineralojik karakterizasyonu için X-ışınları difraktometre (XRD), taramalı elektron mikroskobu (SEM) ve yine aşırı öğütülmüş minerallerin ısıl davranışını gözlemlemek üzere termal analizleri (TGA) yapılmıştır.

2.1 Bulgular ve Tartışma

$CaO + SiO_2 \rightarrow CaO.SiO_2$

tepkimesi göz önüne alınarak; CaO/SiO_2 oranı 1/1,1 olan mermer tozu ve kuvars tozunda hazırlanan öğütülmemiş karışımının XRD analizinde kuvars ve kalsiyum karbonata ait mineralojik izler Şekil 1'de belirgin şekilde izlenmiştir.

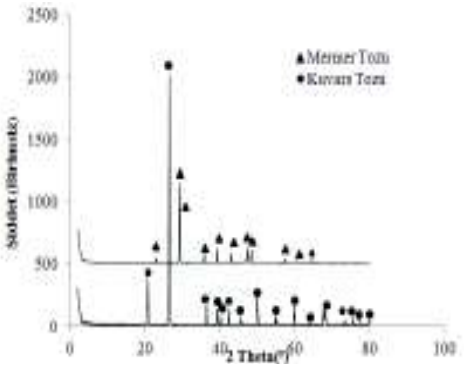

Şekil 1.Mermer tozu ve kuvars tozuna ait XRD desenleri

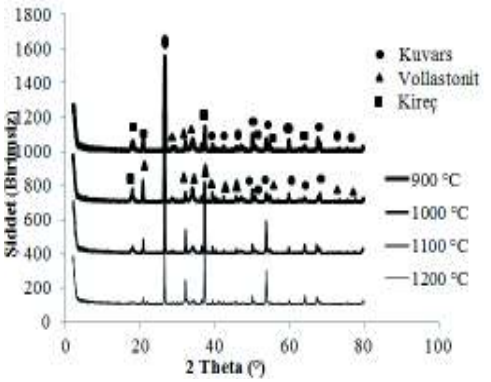

Şekil 2. CaO/SiO_2 oranı 1/1,1 olan mermer tozu ve kuvars tozunda hazırlanan öğütülmemiş mermer tozu- kuvars tozu karışımlarının 900°, 1000°, 1100° ve 1200°C' de 5 saat süre kavrulmaları ile elde edilen ürünlerin XRD desenlerinin karşılaştırılması

Öğütülmemiş karışım malzemeleri tepkimesi amacıyla ön testler yapılmış ve değişik sıcaklıklarda (900, 1000, 1100 ve 1200°C'de) 5 saat süre ile kavurma çalışmaları gerçekleştirilmiştir. Böylece elde edilen ürünlere ait XRD desenleri Şekil 2'de verilmiştir. Buna göre 1000°C'de kavrulma sonucu vollastonit kristalleri görülmeye başlanmış olup, kuvars ve kirece ait pikler belirgin bir şekilde izlenmektedir. Genel anlamıyla kuvarsın kristal yapısını koruduğu gözlenmiştir. Öğütülmemiş karışımın 1200 °C'de 5 saat kavrulmasıyla elde edilen üründe ise kuvars ve kirecin yanında ayrıca vollastonit de bulunduğu görülmektedir. Öğütülmemiş karışım 1100 °C'de kavrulmasına rağmen, her ne kadar XRD analizinde görülmese de, önemli miktarda kalsiyum karbonat ve kireç içermektedir.

Öğütme işleminin mekanik aktivasyona nasıl yol açtığını gözlemlemek amacıyla, seramik sanayinde sır hazırlamada kullanılan

bilyalı jet değirmeni yardımıyla CaO/SiO_2 oranı 1/1,1 olan ve Bilya:Karışım oranı 1/20 olan mermer tozu ve kuvars tozunda hazırlanan karışım çeşitli sürelerde (30', 1, 2, 3, 4, 5 saat) öğütülmüştür. Elde edilen XRD desenleri ise Şekil 3'te verilmiştir.

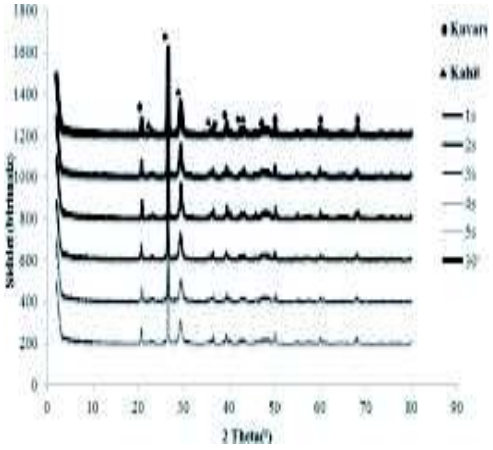

Şekil 3. CaO/SiO_2 oranı 1/1,1 olan ve Bilya: Karışım oranı 1/20 olan mermer tozu ve kuvars tozunda hazırlanan, çeşitli sürelerde öğütülmüş (30', 1, 2, 3, 4, 5 saat süre ile) karışımların XRD desenleri

CaO/SiO_2 oranı 1/1,1 olan ve Bilya: Karışım oranı 1/20 olan mermer tozu ve kuvars tozunda hazırlanan, çeşitli sürelerde öğütülmüş karışımların XRD desenlerinden de anlaşılacağı gibi 30' sürenin mekanik aktivasyon için yeterli olduğu sonucuna varılmıştır. Başka bir deyişle; öğütülmemiş karışıma kıyasla öğütülmüş karışımın XRD desenlerinde kalsiyum karbonata ait piklerin genişliklerinde ise belirgin şekilde bir genişlemenin ve pik şiddetlerinde ise kısalmaların olduğu gözlenmiştir. Böylece yapılan çalışmalarda öğütme işleminin kalsiyum karbonatın kristal yapısını bozarak amorflaşmasına yol açtığı sonucuna varılmıştır. Öğütülmemiş malzemelerin 1000°C'de kavrulması sonucu vollastonit kristalleri görülmeye başlandığı için; 30' öğütülmüş karışım malzemeleri tepkimesi amacıyla 1000 °C'de değişik sürelerde kavurma çalışmaları gerçekleştirilmiştir. Bu doğrultuda; CaO/SiO_2 oranı 1/1,1 olan ve Bilya:Karışım oranı 1/20 olan mermer tozu ve kuvars tozu karışımlarından hazırlanan ve 30' öğütülmüş örneklerinin 1000 °C de çeşitli sürelerde (30', 1, 2, 3, 4, 5 saat) kavrulmasıyla elde edilen ürünlerin XRD analizleri yapılmış ve Şekil 4'te verilmiştir.

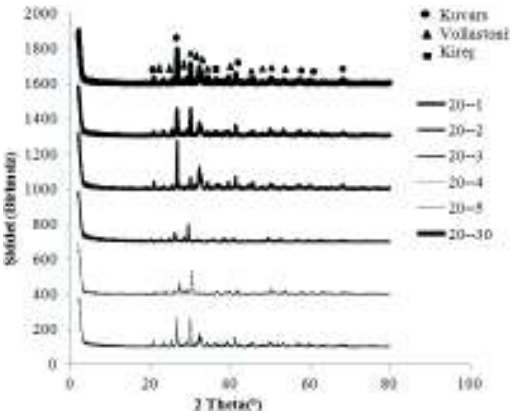

Şekil 4. CaO/SiO_2 oranı 1/1,1 olan ve Bilya: Karışım oranı 1/20 olan mermer tozu ve kuvars tozu karışımlarından hazırlanan ve 30' öğütülmüş örneklerinin 1000 °C de çeşitli sürelerde kavrulmasıyla elde edilen ürünlerin XRD desenleri

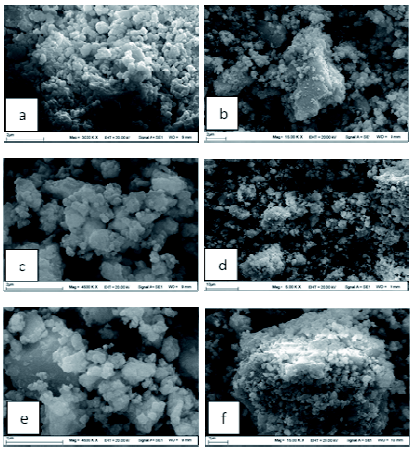

Şekil 5. (a)30', (b)1, (c)2, (d)3, (e)4, (f)5 saat öğütülmüş mermer tozu-kuvars tozu karışımlarının SEM mikrografları

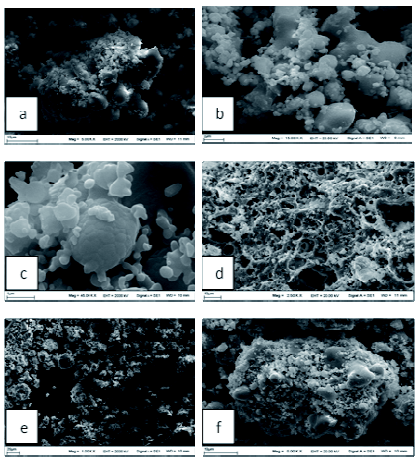

Şekil 6. (a)30', (b)1, (c)2, (d)3, (e)4, (f)5 saat öğütülmüş ve 1000°C'de 30' kalsine edilmiş mermer tozu- kuvars tozu karışımının SEM mikrografları

Bilya:Karışım oranı 1/20 olan mermer tozu ve kuvars tozu karışımlarından hazırlanan ve 30' süre ile öğütülmüş karışımın 1000 °C de 30' kavrulmasıyla elde edilen üründe çok az miktarda kireç bulunmaktadır. Ancak elde edilen ürünün vollastonit olduğu belirlenmiştir.

Öğütülmemiş ve öğütülmüş karışımların 1000 °C'de kavrulmasıyla alınan ürünlerin SEM görüntüleri (Şekil.5. ve Şekil.6.) karşılaştırıldığında öğütülmemiş karışımların 1000 °C'de kavrulmaları sonucu elde edilen ürünlerde kuvars olduğu gibi durduğu, sadece mermer tozunun kalsine olarak üzüm salkımı şeklinde topaklandığı anlaşılmaktadır. Oysa 30 dakika öğütülmüş karışımının 1000 °C'de kavrulması ile elde edilen ürünün SEM fotoğraflarında, mermer tozu ya da kireç ve kuvars tozu görülmemekte, gözenekli yapıdaki vollastonit tanecikleri gözlenmektedir. Yer yer kireçlere de rastlanmakla birlikte, öğütülmüş malzeme 1000°C'de vollastonit oluşturmuştur. Öğütülmemiş karışıma kıyasla öğütülmüş karışımda daha düşük sıcaklıklarda ürün alınabilmektedir. CaO/SiO_2 oranı 1/1,1 olan öğütülmemiş ve Bilya/Karışım oranı 1/20 olan, 30' süre ile öğütülmüş malzemenin 1200-30°C'de 10°C/dak soğutma hızı ile TGA analizi yapılmıştır.

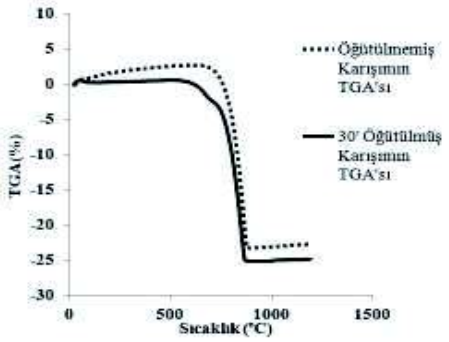

Şekil 7 . 1/1,1'lik karışımdan öğütülmemiş ve Bilya/Karışım oranı 1/20 olan ve 30' öğütülen örneğin TGA grafiği

Termogravimetrik eğrilerin (Şekil 7) karşılaştırılmasıyla, öğütülmemiş karışımın ve 30' süre ile öğütülmüş karışımın dönüşüm sıcaklıklarında belirgin bir şekilde farklılık olduğu görülmüştür. Böylece mermer tozu – kuvars tozu karışımının birlikte öğütülmesi işlemi, vollastonitin oluşum sıcaklığını düşürerek "mekanik aktivasyona" yol açmaktadır.

3 SONUÇLAR

Bu çalışmada, mermer sanayi atığı mermer tozunun kuvars tozuyla birlikte öğütülmesinin, yapay vollastonitin oluşum sıcaklığını düşürerek "mekanik aktivasyona" yol açtığı ortaya çıkarılmıştır. Ancak, yapay üretilen vollastonit ve ticari amaçla kullanılan doğal vollastonit, yer karosu massesi üretimi için belirlenen bir bileşimde ve değişik oranlarda eklenerek, ortaya çıkan seramik ürünlerin teknik özelliklerinin karşılaştırılması gerekmektedir.

Ayrıca, sonraki araştırmalarda, yapay vollastonitin katkısını ortaya çıkarmak üzere pişme sıcaklığı denemelerinin yapılması planlanmaktadır.

KATKI BELİRTME

Bu çalışma, İnönü Üniversitesi tarafından (BAPB Proje 2012/14) desteklenmiştir.

KAYNAKLAR

Andrews, R.W., 1970, Wollastonite, Institute of Geological Sciences, *Mineral Resources*, London.

Baláž, P., Achimovičová, M., 2006, "Mechano-Chemical Leaching in Hydrometallurgy of Complex Sulphide'', *Hydrometallurgy,* (84), 60-68.

Baláž P., 2000, "Extractive Metallurgy of Activated Minerals", *Elsevier*, Amsterdam.

DPT, 2001, Madencilik Özel İhtisas Komisyonu Raporu, Endüstriyel Hammaddeler Alt Komisyonu, *Toprak Sanayi Hammaddeleri 1, Çalışma Grubu Raporu*, Ankara.

Wang, Y., Forssberg, E., 2007, Enhancement of energy efficiency for mechanical production of fine and ultra-fine particles in comminution, *China Particuology*, 5, 193-201 .

Separation of Nanoparticles from Combustion Gases Wastes of Incinerators

A. Neculae, R. Giugiulan, M. Lungu
Faculty of Physics, West University of Timisoara, Bd. V. Parvan 4, Timisoara, Romania

N. Strambeanu
Pro Air Clean Ecologic SA, str. Sulina 5, Timisoara, Romania

ABSTRACT Massively generated in combustion processes the nano-sized particles have received considerable interest in the last years. The separation of the submicron particles into distinct bands, spatially separated one of each other had brought recently considerable attention in many scientific areas. The most promising separation methods are based on dielectrophoresis, phenomenon that induces spatial movement for a neutral particle in a non-uniform electric field, depending on the dielectric properties of the particles and the surrounding medium. This paper investigates the dielectrophoresis capacity to control spatial separation of submicron particles from combustion gases wastes. The concentration of nanoparticle suspension inside a separation device is computed by solving the mathematical model's equations using a finite element code and is characterized using new specific parameters as *recovery* and *purity*. This type of analysis leads to the optimization of the control parameters of an experimental microfluidic device with application in the separation of submicron particles.

1 INTRODUCTION

Nanosized particles have received considerable interest in the past two decades of scientific research. Produced massively from material synthesis and combustion emission, their filtration is an important technological challenge. Another considerable issue for many scientific and technical areas is the separation of nanoparticles in accordance with their physical or chemical characteristics.

Gas resulting from combustion processes contains, besides carbon dioxide and water, finely divided carbon (VOC), carbon monoxide, nitrogen oxides, phosphorous and sulphur, halogenated acids, heavy metal vapors. In addition, in the presence of halogenated acids, through de novo synthesis, VOC and carbon monoxide turn into halogen derivatives of dioxins and furans either found under the form of nanoparticles or adsorbed with the other mentioned compounds on the finely divided carbon, evacuated through the flue gas stream (Minutolo et. al. 2010). All chemical compounds contained in the gas resulting from combustion processes have a toxic effect upon the atmosphere, biodiversity and human organism. These toxic agents spread as nanoparticles or adsorbed on the finely divided carbon, stay in the atmosphere for a long time as very fine suspensions. The harmful effect of nanosuspensions (< 100 nm) has become a more and more pressing issue on a global scale. Their toxicity for human health is relatively high because they can readily enter the human body through inhalation and have a large specific surface area. Once inhaled, infiltrate into the blood very fast and cannot be eliminated, because

the macrophages cells cannot identify them. Recent research has shown that although raw materials may not be dangerous, they can become toxic under the form of nanoparticles (Lungu et. al. 2010). From a public health standpoint, the size of a particle is as important as its composition. Inhaled nanoparticles may generate free radicals, affect the DNA, and alter the genes, which leads to increased cancer risk and incidence of mutagen and teratogenic-related phenomena. The main factors that cause nanoparticle air pollution are industrial emissions (generated by waste incineration plants, metallurgy, cement factories, steam power stations etc.) and internal combustion engines (Rickerby and Morrison, 2007).

Generally, the sources of polluting emissions are equipped with different filters that capture only micron particles, while all nanoparticles escape in the air (Chang and Huang, 2001). Although the nanoparticles mass is smaller when compared with the micron particle mass, the size range of the former is at least for times higher than that of all other masses. Romania has transposed a large part of the European Communities' law in the environmental field. Thus, the Romanian law (Government Decision 541/2003; Order 462/1993 of the Romanian Ministry of Environment and Forests) stipulates that powder emissions are restricted to 30-50 mg/m^3 for large combustion plants and 50 mg/m^3 for other industrial sectors.

The traditional methods attempted for manipulating (retaining and separating) of nanoparticles have not been successful. In the traditional particle-capture device, only a small part of the particles is collected and only when they attach to larger particles. Mechanical devices of controlling particle movement (cyclones, bag filters, sedimentation chambers) are less effective at this scale because of the low weight of the nanoparticles, and the chemical methods are slow and may change the nanoparticles composition during processing. Common Corona electrostatic filters have high micrometric particle retention efficiency (93-99%), but most nanoparticles escape in the air. Flotation separation methods are usually slow and may contaminate the particles under manipulation. Optical techniques sometimes used in trapping nanoparticles have the major disadvantage that they produce significant heating of the fluid that contains the targeted bodies, determining the degradation of the sample (Zhang et. al. 2010, Pethig, 2010).

Nowadays several new methods of particle manipulation are explored. One of the methods utilizing electric fields as the most promising technique for nanoparticle trapping and controlled spatial separation are based on dielectrophoresis (DEP): a phenomenon in which a spatially non-uniform AC or DC electric fields induces a dipolar moment within a dielectric particle that undergoes a DEP motion under the resulted translational force, as in Figure 1. For particles, whose polarizability is greater than the medium the net movement is to regions of highest field strength, whereas particles whose polarizability is less than the medium move to the region of lowest field gradient. This force does not require electrical charged particle; the strength of the force depends strongly on the medium and particles' electrical properties, on the particles' shape and size, as well as on the frequency of the electric field (Pethig, 2010, Neculae et. al. 2012).

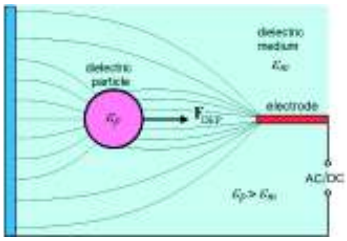

Figure 1. Electrically neutral particle in the presence of a spatially non-uniform electric field. The dipole moment induced within the particle results in a translational force and the dielectric spherical particle undergoes a DEP motion

Due to its capability to separate particles solely according to their dielectric properties

and size (Green et. al. 2002), DEP is used for a wide variety of applications, including separating particles, trapping multiple groups of nanoparticles simultaneously, etc.

In this article, we present a preliminary study regarding the possibility to retain the submicron particles exhausted by combustion gases using dielectrophoresis, to improve the filtering processes. Based on a proposed mathematical model, the concentration of nanoparticle suspension inside a typical separation device is calculated and the performance of the separation device is analyzed in terms of two new specific parameters called recovery and purity, respectively.

The presented results demonstrate that the use of DEP for the manipulation of submicron particles can enhance the performance of filtering devices, in order to reduce of nanoparticles emissions in the air through the optimization of the residual gas filtering conditions.

2 THEORETICAL BACKGROUND

The expression of time averaged DEP force acting on a spherical particle of radius *a* is (Morgan and Green, 2003):

$$\langle \mathbf{F}_{DEP} \rangle = \frac{3}{4}\varepsilon_m K_R(\omega)\nabla\left(|\nabla V_R|^2 + |\nabla V_I|^2\right), \quad (1)$$

$$\bar{K}(\omega) = \left(\bar{\varepsilon}_p - \bar{\varepsilon}_m\right)/\left(\bar{\varepsilon}_p + 2\bar{\varepsilon}_m\right)$$

is the complex Clausius–Mossotti (CM) factor, ω the angular field frequency and $\bar{\varepsilon}_p$ and $\bar{\varepsilon}_m$ are the complex dielectric permittivity of the particle and the medium, respectively. V_R and V_I are the real and respectively the imaginary part of the electrical potential phasor $\bar{V} = V_R + iV_I$, where $i = \sqrt{-1}$. For a homogeneous medium, the electrical potentials satisfy the Laplace's equation:

$$\nabla^2 V_R = 0 \quad \text{and} \quad \nabla^2 V_I = 0. \quad (2)$$

The CM factor not only depends on the dielectric properties of the particle and medium, but also on the frequency of the applied field. The variation in this factor results in a frequency-dependent dielectrophoretic force that is unique to a particular particle type. Therefore, we can use dielectrophoresis as an effective means of separating particles, solely according to their dielectric properties and size. The CM factor is a measure of relative permittivities between the particle and the surrounding medium, and determines the sign of the DEP force. When the sign of $K_R(\omega)$ is positive, the particle is more polarizable than its surrounding medium and are attracted to the locations of electric field intensity maxima and repelled from the minima, phenomenon known as positive dielectrophoresis (pDEP). The opposite occurs when $K_R(\omega)$ is negative, referred to as negative dielectrophoresis (nDEP). Consequently, particles are attracted to regions of stronger electric field when their permittivity ε_p exceeds that of suspension medium ε_m, and are repelled from regions of stronger electric field when $\varepsilon_p < \varepsilon_m$. In summary, can state that pDEP forces cause particles to move towards the regions with the strongest electric field strength, as nDEP forces cause particles to move towards the regions with the weakest field strength.

The macroscopic behavior of a suspension of spherical particles in a dense and viscous fluid can be modeled considering the mechanical equilibrium between an external force **F** and the Stokes drag. When the size of the particles relative to the length of the microchannel and the volume fraction φ of particles are small, the dynamics of the system can be expressed as (Shklyaev and Straube, 2008, Lungu et. al. 2010):

$$\mathbf{v} = \mathbf{u} + \frac{2a^2}{9\eta}\mathbf{F}, \text{ where } : \nabla\mathbf{u} = 0,$$

$$\frac{\partial\varphi}{\partial t} + \nabla\cdot\mathbf{j} = 0, \text{ where: } \mathbf{j} = \varphi\mathbf{v} - D\nabla\varphi. \quad (3)$$

Here **u** and **v** are the fluid and particle velocities, respectively, *a* the particle radius, η the viscosity of the fluid, *t* the time, **j** the particle flux, *D* the diffusion coefficient of the particles and **F** denotes the dielectrophoretic external field.

If the potential, length, time, velocity and particle volume fraction are scaled with V_0, $d, d^2/D, D/d$ and φ_0 (the initial average volume fraction) respectively, the

corresponding dimensionless form of the DEP force is:

$$\langle \mathbf{F}_{DEP} \rangle = F_{0DEP} \nabla' \left(\left| \nabla' V_R' \right|^2 + \left| \nabla' V_I' \right|^2 \right). \quad (4)$$

Here we noted: $F_{0DEP} = (3/4)\varepsilon_m K_R \left(V_0^2 / d^3 \right)$ as a measure of the intensity of the external field, and the transport equations become:

$$\mathbf{v}' = \mathbf{u}' + Q\mathbf{F}', \ \nabla \mathbf{u}' = 0,$$
$$\frac{\partial \varphi'}{\partial t'} + \nabla \cdot \mathbf{j}' = 0, \ \mathbf{j}' = \varphi' \mathbf{v}' - D \nabla \varphi', \quad (5)$$

with: $Q = 2a^2 F_{0DEP} d / 9\eta D$.

The prime symbol above denotes the dimensionless quantities.

Another widely used expression for the intensity of the external field is obtained when a harmonic electric potential $\bar{V} = V_0 \exp(i\omega t - qx)$ is assumed to be imposed at the boundaries of the separation device. V_0 is the amplitude of the electric potential and $q = 2\pi/\lambda$ is the wave number, where λ is the wavelength of the traveling wave. By solving the Laplace equation $\Delta \bar{V} = 0$ the analytical solution for the electric potential can be obtain (Shklyaev and Straube, 2008):

$$\bar{V}(\vec{r}) = V_0 \exp(-iqx) \cosh qy / \cosh qd, \quad (6)$$

and the of the DEP force becomes:

$$\mathbf{F}(\vec{r}) = F_0 \mathbf{F}', \quad (7)$$

where $F_0 = 3\varepsilon_m V_0^2 q^3 k_R / 2\cosh^2(b/2)$ is a parameter related to the intensity of the force field, $\mathbf{F}' = (K' \cosh by, \sinh by, 0)$ corresponds to the term $\mathbf{F}'$ in equation (5), K' is the ratio of the imaginary, K_I, and real, K_R, parts of the Clausius-Mossotti factor and $b = 2qd$ is the so called dimensionless wave number. In the next section, we will present and discuss a set of numerical results obtained in the frame of this mathematical model for describing the behavior of a suspension of spherical particles in a dense and viscous fluid, under the action of an imposed non-uniform external force as in equation (7).

3 NUMERICAL RESULTS AND DISCUSSION

The numerical study deals with the computation of the concentrations field for the nanoparticle suspension subject to the dielectrophoretic force inside a typical separation device. Because the carrying fluid is a gas, only the positive DEP force can act on the suspended nanoparticles. The results are analyzed using two new parameters called *recovery* and *purity*, correlated to the concentration field but more suggestive for the characterization of the separation capabilities of the device.

All the numerical simulations were performed using a partial differential equations solver, FreeFEM++ , based on the finite element method (Neculae et. al. 2012). The schematic representation of the separation device with interdigitated electrode array is presented in Figure 2.

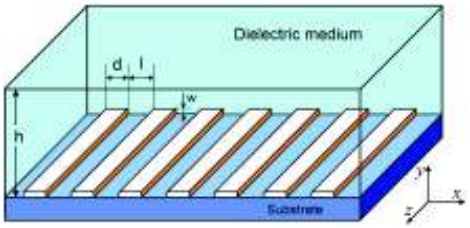

Figure 2. Schematic of the dielectrophoretic-patterning chamber with interdigitated bar electrodes used for DEP separation

For the computation of the DEP force, we solved the Laplace equations (2) for the real and imaginary components of the electric potential, together with the associated boundary conditions. Due to the symmetry of the problem and considering the electrodes long compared to their width, the problem can be treated as two-dimensional. The computational domain and the boundary conditions can be assumed as shown in Figure 3, where the particular case d=l=100μm, and h=2d was considered. Each electrode was assigned its corresponding value for the real part of the potential phasor. Similar boundary conditions hold for the imaginary part of the potential phasor (Lungu et al 2010).

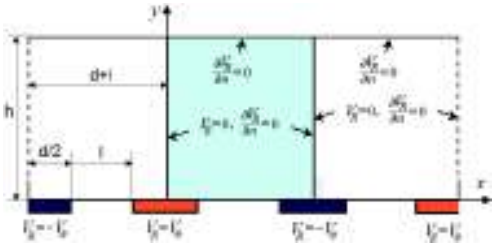

Figure 3. The geometry of the computational domain and the boundary conditions for the real part V_R of the electric potential. The solid lines indicate the basic unit cell

Details on the validation procedure of the program and an analysis of the dielectrophoretic force distribution are given in (Neculae et. al. 2012).

The simulations were performed for a suspension of particles with characteristic size a=200nm in water ($\eta = 10^{-3}\,\mathrm{kgm^{-1}s^{-1}}$, $\rho = 10^{3}\,\mathrm{kgm^{-3}}$, $D \approx 10^{-12}\,\mathrm{m^2s^{-1}}$, ε_m ≈ 80). For a real part of the CM factor $K_R \approx 0.6$, an amplitude of the electric potential V_0 ≈ 1V and a traveling wave with $\lambda = 400\mu\mathrm{m}$, we obtain for the dimensionless parameter in equation (5) a typical value of $Q \approx 0.2$ and a value $b = \pi$ for the dimensionless wave number.

The computations of concentration distribution inside the device were performed for values of the parameter Q ranging from 0.1 to 10. We remind here that the key parameter of the problem Q can be practically varied by modifying the applied signal. Thus, by increasing or decreasing the voltage, Q increases or decreases corresponding to a square law. For the sake of simplicity, we drop the prime symbol, even the analysis is performed in terms of dimensionless quantities.

The results obtained for the magnitudes of the vector $\nabla'\left(\left|\nabla' V_R'\right|^2 + \left|\nabla' V_I'\right|^2\right)$, proportional to the dimensionless DEP force given by equations (5), are presented in Figure 4. The area shown corresponds to the region with $y < 100\mu\mathrm{m}$, the magnitude of the DEP forces above this level being negligible.

Figure 4. Calculated values for the magnitudes of the dimensionless DEP force, plotted on logarithmic scale: $\langle \mathbf{F}_{DEP} \rangle / F_{0DEP}$

One observes a periodic variation for both vectors; the magnitudes of the computed quantities increase to a maximum value at the electrode edge and diminish rapidly with distance in the vertical direction. This periodic distribution of the potential allows for an analytical solution for the DEP problem to be found.

The computational domain consists of a rectangular domain with two rows of electrodes of negligible geometry (Fig. 5), with a harmonic electric potential is imposed at the boundaries.

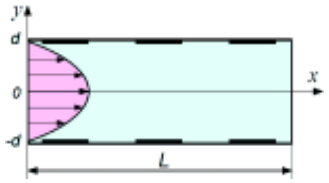

Figure 5. Analytical setup with simplified geometry used for simulations

When the geometry of the electrodes is neglected, the flow field is described by a classical Poiseuille profile. The influence of the velocity field is not analyzed here, so we considered in all computations a typical value of 10 μm/s for the maximum flow velocity.

In order to simulate the behavior of a suspension subjected to dielectrophoretic force, the system of equations (5) for the force given by equation (5) is solved for different values of the parameter Q, corresponding to different intensities of the dielectrophoretic force.

The cconcentration field computed in the simplified domain for the parameter $Q = 1$ is

presented in Figure 6:

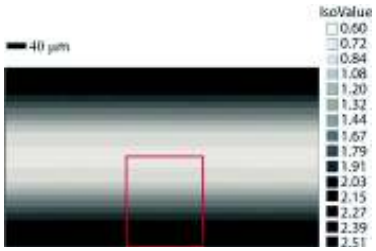

Figure 6. Concentration field computed for $Q = 0.2$

The simulation shows that the particles are attracted to the electrodes due to the pDEP effect. From a practical point of view, it is obvious that if we are interested in the efficient recovery of the suspended particles, the recovery process must take place in the region of enriched fluid. We consider that the recovery device is placed in such a manner that it separates a region of height h (outlet) measured from the electrodes and so we collect the fluid with a higher particle concentration. Figure 7 shows the detail from Figure 6 with the region of interest (left) and the recovery zone (right).

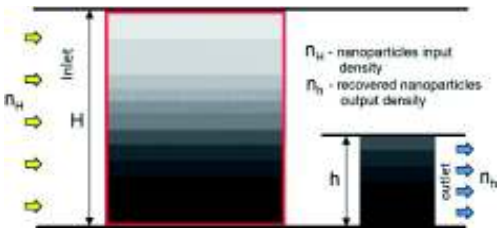

Figure 7. Detail with the recovery zone

To obtain an efficient separation we must collect as much of the particles from the fluid suspension as possible, which on one hand demands a small value for h in order to separate highly concentrate fluid, and on the other hand a large value for h, in order to better collect the particles.

For the analysis of the separation process we define a set of parameters describing this process, related to the concentration distribution:

- the recovered mass – *Recovery* (R):

$$R = \int_0^h C(y)dy \tag{8}$$

- the particle density (n):

$$n_h = (1/h)\int_0^h C(y)dy \tag{9}$$

- the *Purity* (P):

$$P = \frac{n(h) - n_0}{n_{\max} - n_0} \tag{10}$$

where h is the outlet width ($0 \le h \le H$) and $n_0 = 1$ is the value of the parameter *Purity* in absence of dielectrophoretic force.

Next, we discuss the significance and the behavior of these parameters in the context of the considered problem.

In Figure 8 we presented a typical distribution of the concentration field, for different outlet widths and DEP force intensities.

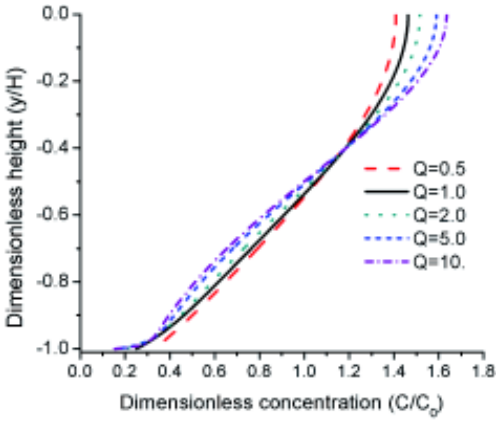

Figure 8. Distribution of the concentration, for different outlet width and DEP force intensities

For all DEP force intensities the calculated concentration field reach its maximum at h=0 (near the electrodes) and its minimum at h=H (in the center of the device). As expected, the maximum value of the concentration field increases with the intensity of the DEP force.

Based on this computed concentration field we can calculate the variation of the parameters (8)-(10).

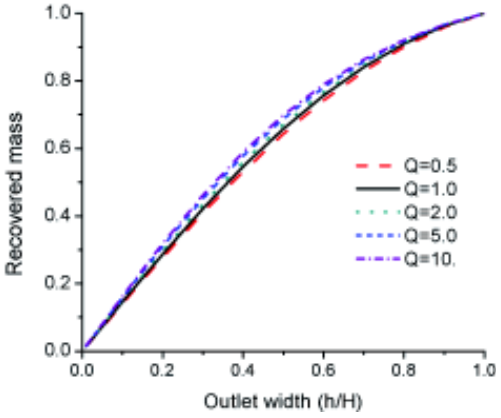

Figure 9. Distribution of the recovered mass (*Recovery*) for different outlet width and DEP force intensities

The behavior of the *Recovery* (R) as a function of the outlet width is presented in Figure 9. This parameter presents a continuous increasing with h, corresponding to the increasing quantity of mass contained in the separation region.

On the other hand, the calculated particle density diminish with h, as shown in Figure 10, where we presented the distribution of the particle density (9) for different outlet width h and DEP force intensities Q.

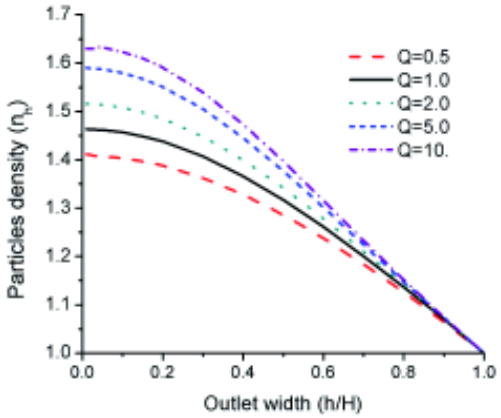

Figure 10. Distribution of the particles density for different outlet width and DEP force intensities

This two opposite trends are better outlined in Figure 11, where we showed the variation of parameters recovery and purity, at a intensity of the dielectrophoretic forces $Q=1$ (similar behaviors are obtained for all values of Q).

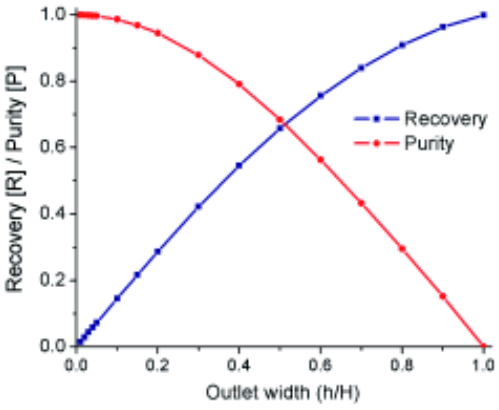

Figure 11. *Recovery* and *Purity* for different outlet width, at $Q=1$

The main conclusion we can extract from the results presented in Figure 11 is that we can find a value of the outlet width which is a good compromise between the quantity of recovered mass and purity of separated material. In all computations we performed in the frame of the presented mathematical model and geometry we obtained a value of $h \approx 0.5H$.

This type of simulations performed for different geometries can help to find the correct dimension of the recovery device and consequently can lead to the optimization of the dielectrophoretic device.

CONCLUSIONS

The study presented in this paper focuses on the description of submicron particle behavior in a suspension under the action of DEP forces. More precisely, the concentration profile of the particles exposed to DEP forces is numerically computed and the separation efficiency (evaluated in terms of recovery and purity) of the device is analyzed. The mathematical modelisation and the numerical simulations

can help us both understand the physics and behavior of dielectrophoresis as well as allow us to design new and more efficient devices for submicron particle sorting. The results reveal that the nanoparticles in suspension tend to concentrate on the channel walls depending on their properties (nature, size), by adjusting the applied voltage at the command electrodes. The parameters *Recovery* and *Purity* give a global image of the influence of the simulation parameters on the separation process.

ACKNOWLEDGMENTS

This work was supported by a grant of the Romanian National Authority for Scientific Research, CNCS – UEFISCDI, project number PN-II-ID-PCE-2011-3-0762.

REFERENCES

Chang, M and Huang, C, 2001. Characteristics of Energy Flow in Municipal Solid Waste Incinerator, *J. of Environ. Eng.,* 127, pp.78–81.

Green, NG, Ramos, A and Morgan, H, 2002. Numerical solution of the dielectrophoretic and travelling wave forces for interdigitated electrode arrays using the finite element method, *J. of Electrostatics,* 56, pp.235-254.

Lungu, M, Neculae, A and Bunoiu, M, 2010. Some considerations on the dielectrophoretic manipulation of nanoparticles in fluid media, *J. of Optoelectronics and Advanced Materials,* 12, pp.2423-2426.

Minutolo, P, Sgro, L, Costagliola, M, Prati, M, Sirignano, M and D'Anna, A, 2010 Ultrafine particle emission from combustion devices burning natural gas, *Chem. Eng. Trans.,* 22, pp.239-244.

Morgan, H and Green, N, 2003. *AC Electrokinetics: Colloids and nanoparticles* Research Studies ltd. Baldock, Hertfordshire, 340 p.

Neculae, A, Biris, C, Bunoiu, M and Lungu, M, 2012. Numerical analysis of nanoparticles behaviorin a microfluidic channel under dielectrophoresis *J. Nanopart. Res.,* 14, pp.1-12.

Pethig, R, 2010. Review Article—Dielectrophoresis: Status of the theory, technology, and applications, *Biomicrofluidics,* 4, pp.022811-1 – 02281-34.

Rickerby, D and Morrison, M, 2007. *Report from the Workshop on Nanotechnologies for Environmental Remediation*, JRC Ispra, http://www.nanowerk.com/nanotechnology/reports/reportpdf/report101.pdf.

Shklyaev, S and Straube, A, 2008. Particle entrapment in a fluid suspension as a feedback effect, *New Journal of Physics*, 10, pp.1-12.

Zhang, C, Khoshmanesh, K, Mitchell, A and Kalantar-Zadeh, K, 2010. Dielectrophoresis for manipulation of micro/nanoparticles in microfluidic systems, *Anal. Bioanal. Chem.*, 396, pp.401–420.

Scale-Up of Crushing Tests

J. A. M. Luz, F. O. Milhomem
Federal University of Ouro Preto, Brazil

ABSTRACT Scale-up is a recurring problem in metallurgical testwork. Crushing operation has been scaled up usually by engineering practice criteria for crusher sizing, or comparison procedure. This article shows a more tenable method for jaw crusher sizing. It comes from generalization of the product size distribution curves as a function of opening size of the jaws. Gates-Gaudin-Schumann equation was successfully employed to fit manufacturer's data. In order to apply the method a bench scale crushing campaign was carried out using gneiss lumps as material to be comminuted. Moreover, sample characterization was performed as a supplement, aiming to determine properties relevant to a study of comminution and allow any further corroboration of experimental data as well. Schmidt's impact hammer was used to compressive strength measurement, obtaining average of 28.15 MPa for rock samples. Bond's work index of gneiss sample has resulted 46,8 kJ/kg. Rosin-Rammler equation displays higher statistical correlation than does Gates-Gaudin-Schumann equation for product size distribution with respect to gneiss, complicating but not preventing the scale-up procedure here preconized.

1 INTRODUCTION

Crushability curves of gneiss were obtained from crushing batch tests carried out employing a lab scale jaw crusher and rock samples coming from Barbacena municipality, in Minas Gerais State, Brazil. Methods and operational conditions adopted for this experimental campaign were described later in this paper. Sample characterization effort was also undertaken, in order to clearly describe the main properties of the system under study (allowing whether criticism to results or occasional experimental corroboration thereof).

Size distribution of crushed material was simulated for a hypothetical industrial scale with flowrate of 80 metric tons per hour.

The following possible products were taken into account for such a hypothetical production, in order to use them as aggregates in building construction sector, according to Brazilian standard specifications:

- Powder stone: particles below 4.6 mm;
- Gravel # 0: particles below 12.5 mm;
- Washed Gravel # 0 (fine): particles below 19.5 mm;
- Gravel # 1: particles between: 12.5 mm and 19 mm;
- Gravel # 2: particles between: 19.0 mm and 32.0 mm;
- Gravel # 3 (ballast): particles between: 32.0 mm and 64.0 mm;
- Gravel # 4: particles between: 64.0 mm and 76.0 mm.

2 MATERIALS AND METHODS

2.1 Samples and Sample Characterization

Gneiss boulders used for this study were obtained by drilling and blasting the outcropping ore at site (industrial exploitation has not yet begun). The resulted fragments had tabular shape, as displayed in figure 1. In that figure the scale's minor tick marks refer to millimeters and the vertical scale has 7 cm. Particle sizes can be evaluated from shadow ratio between vertical scale and fragments.

Figure 1. samples as received

In total 142.4 kg was used for the tests. Descriptive statistics of sample lumps is summarized in following table.

Table 1. Descriptive statistics of gneiss lumps

Average mass	3.75 kg
Standard error	0.4927 kg
Median	2.74 kg
Mode	2.76 kg
Standard deviation	3.037 kg
Variance	9.233 kg
Kurtosis	1.979
Skewness	1.576
range	12.8 kg
Minimum	0.62 kg
Maximum	13.42 kg
Sum	142.43kg
Count	38 lumps

Concomitantly to crushing tests a Schmidt hammer (sclerometer) was employed to determine mechanical strength of 21 stone lumps, in order to evaluate the sample stiffness. Measurements were taken under two classes for these experiments, namely:

1. Measurement with the sclerometer axis orthogonal to the sample's apparent schistosity;
2. Measurement with the sclerometer axis parallel to the sample's apparent schistosity.

The resistance inference was made from the rebound (read directly in the instrument scale) and employing the appropriate chart. The measurements were performed with the axis of Schmidt hammer vertically downward (corresponding to the angle of 90°, in the manufacturer's conversion charts) on sample's flatter faces. The figure 2 displays the features of this kind of sclerometer (taken from Luz & Segato, 2005).

Figure 2. Schmidt hammer (N type - 2.207 Nm impact energy) with retractable impact plunger at starting and ending position (locked by pressing the pushbutton after impact, allowing scale reading).

2.2 Bond's Work Index (wi) Estimation

The method of comparative ***wi*** due to Berry and Bruce as quoted by Wills & Napier-

Munn (2006) was used to evaluate in a simplified way the behavior of the sample to comminution. In this work the reference material of known grindability was agalmatolite. The reference material was ground for 300 s. An identical weight of the test ore was then ground for the same time interval and under the same operational conditions such that the energy consumed in grinding was identical with that of the reference ore. Then work index of gneiss under test could be estimated from Bond's Equation. As the specific crushing energy is the same the following equation holds:

$$10 \times wi_{ref} \times \left[\frac{1}{\sqrt{P_{80ref}}} - \frac{1}{\sqrt{F_{80ref}}} \right] = 10 \times wi_{gneiss} \times \left[\frac{1}{\sqrt{P_{80gneiss}}} - \frac{1}{\sqrt{F_{80gneiss}}} \right] \quad (1)$$

Where: ***wi*** – crushing work index [J/kg]; P_{80} – sieve size passing 80 % of the crusher product [μm]; F_{80} – sieve size passing 80 % of the crusher feed [μm]. Subscript ***ref*** stands for "reference material" (agalmatolite from Pará de Minas municipality in Minas Gerais State, Brazil)

The agalmatolite work index was wi_{ref} = 69,12 kJ/kg (19,2 kWh per metric t).

After determination by sieving of the size distributions of feed and product the only unknown in precedent equation is the gneiss work index (wi_{gneiss}).

The following table summarizes the experimental conditions of dry grinding tests made for determining the work index of gneiss sample.

Table 2. Operational conditions for grinding tests

	Agalmatolite	*Gneiss*
Equipment	Ball mill	Ball mill
Effective mill diameter	0,22 m	0,22 m
Grinding media	Steel balls	Steel balls
Ball diameter	According to Bond standard test	According to Bond standard test
Number of balls	285	285
Mass of balls	20,125 kg	20,125 kg
Critical velocity fraction	70 %	70 %
Time	300 s	300 s
Feed size (F_{80})	1,32 mm	1,36 mm
Product size (P_{80})	0,32 mm	0,21 mm

2.3 Crushing Tests

The head sample was firstly broken up by hand with use of a sledge hammer (resulting top size was about 75 mm). Secondly the lumps were crushed in a single toggle jaw crusher. Two batch tests were carried out and their operating conditions are summarized in the following table 3:

After each crushing test, broken ore was sieved on vibrating screens, in three sequential sieving steps (retained material in the bottom pan of the first step was the feed for the second one, and retained material in the bottom pan of the second sieving was the feed for the third step).

Table 3. Operational conditions for crushing tests

	First crushing test	Second crushing test
Equipment	Jaw crusher	Jaw crusher
Open-side setting	20 mm	7 mm
Closed-side setting	10 mm	2 mm
Gape x width	130 x100 mm^2	130 x100 mm^2
Eccentricity jaw frequency	10 mm 6 Hz	10 mm 6 Hz

The following screen openings were used for particle size analysis on each screening:

- First sieving (dry): 25.4 mm, 19.1 mm, 12.7 mm, 6.3 mm, 4.7 mm, and bottom pan;
- Second sieving (wet): 3.34 mm, 2.36 mm, 1.67 mm, 0.836 mm, and 0.418 mm, and bottom pan;
- Third sieving (wet): 0.209 mm, 0.148 mm, 0.105 mm, 0.740 mm, 0.530 mm, and bottom pan.

3 RESULTS AND DISCUSSION

3.1 Particles Morphology

The following figures 3 and 4 shows the progeny morphology generated by the crushing test, in different openings obtained by sieving.

Figure 3. At the right, material retained on 25.4 mm; at left, material between 6.3 mm and 4.7 mm

An expeditious mineralogical inspection of fresh surfaces (like the one showed in figure 4) has revealed the presence of quartz and plagioclase among the leucominerals as well as the occurrence of a mafic phase (probably an inosilicate, not biotite that is a phyllosilicate)

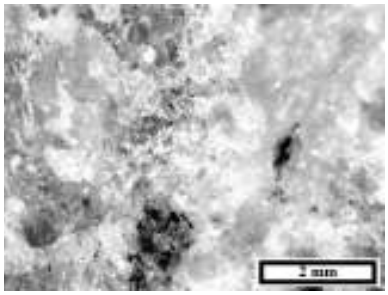

Figure 4. Micrograph of a fresh surface of gneiss fragment

3.2 Mechanical Strength

The compressive strength analysis by Schmidt hammer is shown in the following table. Low rock resistance was observed. Perhaps it is because Schmidt hammer is very error prone, although its great advantage is that it is very fast in getting results (Aydin, 2009).

Table 4 presents the results of samples' mechanical strength.

Table 4. Compressive strength analysis of gneiss samples

Compressive strength- orthogonal to schistosity		
Mean [MPa]	Standard deviation [MPa]	Coefficient of variation [%]
30.42	12.305	40.45
Compressive strength- parallel to schistosity		
Mean [MPa]	Standard deviation [MPa]	Coefficient of variation [%]
25.88	11.954	46.19
Compressive strength- mean values		
Mean [MPa]	Standard deviation [MPa]	Coefficient of variation [%]
28.15	12.295	43.68

3.3 Bond's Work Index of Gneiss

Bond's work index for the sample under analysis has resulted the value of 46,82 kJ/kg (13,01 kWh/t) obtained by comparative method.

3.4 Crushability Curves for Gneiss

Usually crusher is sized from standard crushability curves previously carried out by crusher manufacturers and shown in their catalogs (Utley, 2002). Such curves were obtained empirically, generally employing aphanitic rocks like basalt or limestone. Crushability curves corresponding to the industrial crusher type under analysis are shown in the figure 5 (each curve corresponds to a specific CSS – closed-side setting; expressed in millimeters).

These curves can be described theoretically displaying adequate statistical correlation by statistical distribution curves of Gates-Gaudin-Schumann (Luz, 2011).

The Authors have treated mathematically catalog data (Metso, 2005; similar to Metso, 2012) for single toggle jaw crushers (series C, Nordberg), obtaining the following general equation for the cumulative passing, against to the opening in crusher closed-side setting (CSS; expressed in same dimension unity that one for particle size, d_p):

$$Y_p = \left(\frac{d_p}{1.423 \times CSS} \right)^{0.898} \quad (2)$$

Taking up knowledge on CSS and jaw movement or throw (given for each crusher), calculation for opening in the open jaw position (OSS – open-side setting) is trivial. The throw is done as function of crusher gape (G, given in meters) by Gupta and Yan (2006):

$$T = OSS - CSS = 0.0502 \times (G)^{0.85} \quad (3)$$

The sieve analyses of crushed gneiss under the two CSS values tested are shown in figure 6.

However, particle size analysis data for the crushed products has revealed low statistical adherence to the classical Gates-Gaudin-Schumann equation. Their size analysis has showed better statistical correlation with the Rosin-Rammler distribution

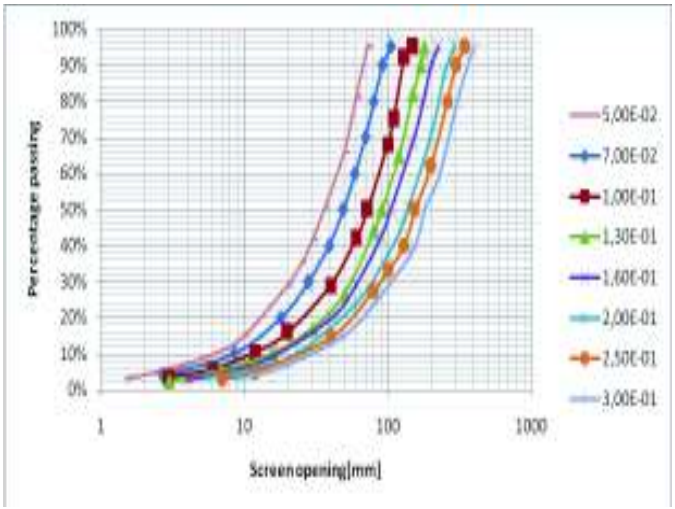

Figure 5. Standard product curve of Nordberg C jaw crusher

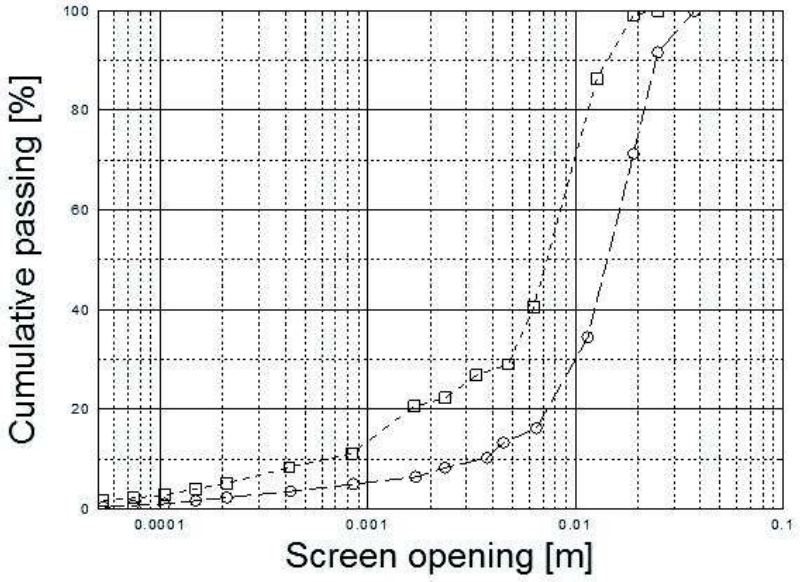

Figure 6. Size reduction curve of gneiss under study. Squared plot markers stand for CSS = 7 mm and OSS = 2 mm; circle plot markers stand for CSS = 10 mm and OSS = 20 mm

The Rosin-Rammler distribution, expressed in terms of median diameter (d_{50}) is given by equation 4:

$$Y_p = 1 - \exp\left[\ln\left(\frac{1}{2}\right) \times \left(\frac{d_p}{d_{50}}\right)^n \right] \qquad (4)$$

Where: Y_p represents the cumulative fraction finer than d_p that is the particle diameter (or sieve opening) and n is the sharpness of distribution.

The statistical treatment of the data in coarse screening series (most representative of crushing) has showed the following values summarized in table 5.

Table 5. Regressional results for crushing tests

	First test	Second test
Median size (d_{50})	0.0141 m	0.007 m
Sharpness	2.015	1.775
Correlation: R^2	99.36 %	99.96 %

One can see from the above data that reproducibility was good, since statistical residues did not display significant bias.

As a matter of fact, there was discrepancy between the size distributions from catalog data and those from the results described in this study (obtained from laboratory crushing testwork). This discrepancy hampers the predictability of results to be expected on an industrial scale application.

However, we can adopt a premise for any material whose properties are not too much discrepant from those of basalt and limestone. This assumption is that for the same value of CSS (and same value of OSS)

the product top size it will be the same. Top size hereafter is nominally adopted as the d_{98} (ie: that opening sieve through which 98 % of the crushed material will pass).

The preconized premise is crucial for the scale up procedure here developed.

Thus, taking the average sharpness value (n = 1.895) for the generic size distribution of crushed gneiss it leads to following equation:

$$0.98 = 1 - \exp\left[\ln\left(\frac{1}{2}\right) \times \left(\frac{d_{98}}{d_{50}}\right)^{1.895}\right] \quad (5)$$

On the other hand equation 6 also holds as a consequence of the adopted scale up criterion:

$$0.98 = \left(\frac{d_{98}}{1.423 \times CSS}\right)^{0.898} \quad (6)$$

Equaling equations 5 and 6 after simple algebrism, having eliminated the value of d_{98} in the above expression, and adopting industrial crushing with CSS = 50 mm (just as a convenient example) one gets the equation 7, which allows forecasting of product median diameter in the considered industrial scale gneiss crushing operation:

$$d_{50\,gneiss} = \left[\frac{\ln\left(\frac{1}{2}\right)}{(1-0.98)}\right]^{\frac{1}{n}} \times 0.070 = 0.028 \text{ m} \quad (7)$$

Therefore, it entails equation 8 for particle size distribution due to the industrial crushing for gneiss under study:

$$Y_p = 1 - \exp\left[\ln\left(\frac{1}{2}\right) \times \left(\frac{d_p}{0.028}\right)^{n}\right] \quad (8)$$

Figure 7 displays the product grain size distribution of gneiss with respect to lab tests and predicted industrial scale.

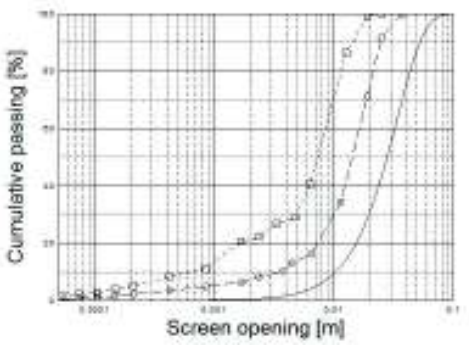

Figure 7. Crushability curve for gneiss; solid line curve was obtained by equation 5 (industrial scale); square plot markers stand for CSS = 7 mm and OSS = 2 mm; circles plot markers represent CSS = 10 mm and OSS = 20 mm

3.5 Scale-Up For Jaw Crusher

One example for the equation use is for scale up a jaw crushing operation with catalog capacity of 80 t/h. For the case in question, one can propose a single toggle jaw crusher with opening of 800 mm x 510 mm, for instance, like a Nordberg C80 crusher (with nominal power of 75 kW). Its catalog capacity is 80 metric tons per hour, when working in open circuit mode (just for simplicity) and under the previously adopted CSS value. The chosen crusher will generate a product mix approximately equal to that shown in table 8.

Table 6. Crushed gneiss mix for the simulated jaw crusher

Gravel	Top Size [m]	Min. size [m]	Proportion [%]	Production [t/h]
Gravel 0:	0.0125	0	14.03	11.2
Gravel 1:	0.0190	0.013	14.39	11,5
Gravel 2:	0.0320	0.019	30.84	24.7
Gravel 3:	0.0640	0.032	37.20	29.8
Gravel 4:	0.7600	0.064	3.54	2.83
Total:			100.00	80.0

Generally speaking with respect to crushing capacity, it should be borne in mind that jaw crushers work effectively in half the jaw reciprocating cycle and inside the full crushing cavity or chamber. The equation which provides the volumetric flow rate, Q_v (in m³/h) feed jaw crusher is given by:

$$Q_V = \frac{(OSS + CSS)}{2} \times \frac{(OSS - CSS)}{tg\alpha} \times L \times 60 \times N \times k = \frac{(OSS^2 - CSS^2)}{2 \times tg\alpha} \times L \times 60 \times N \times k \quad (9)$$

Where: ***OSS*** - jaw opening in the open position [m]; ***CSS*** – jaw opening in the closed position [m]; $\boldsymbol{\alpha}$ – nip angle [°]; ***L*** – effective width of crushing chamber [m] , ***N*** – angular velocity of the crusher flywheel [rpm]; ***k*** – empirical coefficient depending on the material and equipment [-].

The coefficient ***k*** takes into account both bulk swelling of the broken material and friction at its fall, besides of additional geometric effect of jaw's tooth profile (in closed position). Usually ***k*** ranges from 0.4 to 0.45 and nip angle generally falls in the range between 19° and 23°, according Galperin et al. (1982).

Once calculated the size distribution of industrial scale crusher, the previous equation allows forecasting the actual hourly capacity of scaled up crusher in case of lack of manufacturer data.

On the other hand, power consumption of comminution operation can be estimated by classical Bond equation (Utley, 2002; Beraldo, 1987). However, this procedure has suffered criticism when it comes to crushing.

One of the recent propositions was preconized by Magdalinovic, which is a modification of Bond's approach. Specific crushing energy is expressed by Magdalinovic as (Jankovic et al, 2005):

$$E = 10 \times \frac{A}{\sqrt{P_{80}}} \times wi \times \left[\frac{1}{\sqrt{P_{80}}} - \frac{1}{\sqrt{F_{80}}} \right] \quad (10)$$

Where: ***A*** –material and crusher dependent parameter [$(\mu m)^{1/2}$]; ***wi*** – crushing work index [J/kg]; $\boldsymbol{P_{80}}$ – sieve size passing 80 % of the crusher product [μm]; $\boldsymbol{F_{80}}$ – sieve size passing 80 % of the crusher feed [μm].

In equation 10, the dimension of ***E*** is J/kg. Once in possession of the actual value of specific energy, scaling up for industrial conditions is a straightforward procedure.

4 CONCLUSION

Crushability of sample under study is such that the theoretical distribution of Rosin-Rammler applies better than Gates-Gaudin-Schumann, often preconized for most commonly occurring granular products of crushing systems.

The crushing strength exhibited high coefficient of variation indicating the compositional variation in spot gneiss

studied. Strength results show that the rock in question is fully satisfactory as aggregate for concrete and other structures in the construction industry.

The nominal product mix in a hypothetical industrial scale recorded here was based firstly on the validity of the assumption that whatever a given material fed into the crusher the product top size will be approximately equal, provided the crusher is the same and operating with the same CSS (and hence the same OSS). As main scale up criterion it is of paramount importance to keep in mind that this would be valid regardless of the type of particle size distribution of material (i.e.: even though there are no equal particle size distributions).

The second premise for crushing system scale up is that the sharpness parameter of crushability curves is kept constant (the perceivable "parallelism" of the crushability curves of manufacturers' charts testifies in favor of this principle).

Although very likely in reality it would be useful to check empirically the validity of these assumptions here adopted. Such validation is beyond the scope of the present work since it would require several crushing tests on an industrial scale, not yet carried out by the authors to date.

As a final point, it should be noted that the scale up procedure recommended here has the potential to be applied not only to the system under study, but to common types of non-friable materials or ores. Of course, the fact of the present work have been based on empirical correlations do not rob per se its validity as a method to scale up. Friable materials, however, almost certainly will behave in a manner inconsistent with the premises here adopted.

The authors express their gratitude to engineer Adhebar Soares Jr. and Mr. Antônio C. Torres for their help in running some experiments. The authors also thank *CNPq*, *Capes*, *Fapemig* and *Gorceix Foundation* for supporting this research.

REFERENCES

Aydin, A, 2009, ISRM Suggested method for determination of the Schmidt hammer rebound hardness: Revised version, *International Journal of Rock Mechanics & Mining Sciences*, V. 46, pp. 627–634.

Beraldo, J. L. (ed.), 1987, *Moagem de Minérios em Moinhos Tubulares*. Edgard Blücher, São Paulo, 143 p.

Galperin, M. *et alii*, 1982, *Construction Equipment,* Mir, Moscow.408 p.

Gupta, A.; Yan, D. S., 2006, *Mineral Processing Design And Operation: An Introduction*, Esevier, Amsterdam, 694 p.

Jankovic, A; Valery, W.; Davis, E., Cement Grinding Optimisation. *Minerals Engineering*, V. 17 (2004), pp. 1075–1081.

Luz, J. A. M., 2011, *Fracionamento Granulométrico de Sistemas Particulados*. Ouro Preto, 126 p.

Luz, J. A. M. & Segato, M. C. (Ed), 2005, Caracterização geomecânica expedita de rochas ornamentais, *Anais do XXI Encontro Nacional de Tratamento de Minérios e Metalurgia Extrativa*. V. 02, pp. 509 - 516.

Metso Minerals, 2005, *Manual de britagem*, Allis Mineral Systems, São Paulo.

Metso Minerals, 2012, *Nordberg C Series jaw crushers (Brochure No. 1005-05-12-ESBL)*. Metso Minerals, Tampere, 24 p.

Utley, R. W. 2002, Selection and Sizing of Primary Crushers. In: *Mular A. L.; Halbe, D. N.; Barratt D. J. (ed.), 2002, Mineral Processing Plant Design, Practice, and Control: Proceedings - Volume 1,* SME, Littleton, pp. 584 - 605.

Wills, B.; Napier-Munn, T. J., 2006, *Will's Mineral Processing Technology (7th ed.)*. Burlington: Butterworth-Heinemann, 2006.

Investigation of Some Parameters Affecting the Ultra–Fine Grinding of Refractory Silver Ore Tailings by Stirred Mill

O. Celep, E. Y. Yazıcı
Karadeniz Technical University, Department of Mining Engineering, Trabzon

ABSTRACT In this study, ultra-fine grinding of a refractory silver ore tailings was studied. A laboratory scale pin–type vertical stirred mill and ceramic beads were employed for the grinding tests. The effects of ball diameter (2–4.5 mm), stirring speed (200–800 rpm) and ball charge ratio (50–80%) on the particle size (d_{80}, μm) of the ground material and energy consumption were investigated. Finer products were obtained by increasing the stirrer speed and ball charge ratio. Larger balls produced coarser products. These tests showed that under the suitable conditions of stirrer speed, ball diameter and ball charge ratio, particle sizes (d_{80}) of <5 μm can be achieved over 15 min. grinding time. Preliminary cyanidation tests also showed that ultra-fine grinding process using pin–type vertical stirred mills could be used as a physical pretreatment method prior to cyanide leaching to improve the leaching recoveries of silver from the refractory silver tailings.

1 INTRODUCTION

Refractoriness of gold and silver ores is mainly arised from the encapsulation of fine gold or silver particles within sulphide (e.g. arsenopyrite and pyrite) and gang minerals in that these particles are not accessible to the lixivianting action of cyanide and oxygen (La Brooy et al., 1994; Marsden and House, 2006). Ultra–fine grinding (UFG) as a environmentally sound and low cost physical method can be suitably used to liberate the encapsulated gold in particle sizes between 1–2 μm to approximately 20 μm (Corrans and Angove, 1991; Celep et al., 2011). Ultra–fine grinding is a viable alternative to conventional oxidative pretreatment methods such as roasting, pressure oxidation and bio–oxidation which have been commercially practiced to enhance gold/silver recoveries from refractory ores (Dunn and Chamberlain, 1997; Gunyanga et al., 1999; Ciftci and Akcil, 2010).

Ultra–fine grinding (UFG) of minerals down to a few micrometers are widely practiced by stirred media mills e.g. Vertimill®, Stirred Media Detritor (SMD®) and ISAMill®. (Jankovic and Valery, 2004; Sepulveda, 1981). Different types and sizes of grinding media are available for a range of feed material and size (Jankovic, 2003).

Many process parameters such as stirrer speed, ball diameter and ball charge ratio contribute to the performance of a grinding process (Jankovic, 2003). There are many studies available which investigated the operating parameters affecting the grinding performance of stirred media mills (Tüzün et al., 1995; Zheng, J., 1997). Significant parameters affecting comminution process and stress intensity in the stirred mills are reported as mineral type, specific energy input, bead size and load volume (Orumwense and Forssberg, 1992; Kwade, 1999). Small grinding media should be used to obtain a fine product. However, when the

media size becomes too small, grinding becomes less efficient (Lichter and Davey, 2006; Gao and Holmes, 2007). High density media has a better performance over low density media (e.g. glass, ceramic, pebble etc.) on grinding coarse materials at low speeds. Stirrer speed is also known to be one of the most important factors in the stirred media milling (Zheng, 1997).

In this study, the effects of parameters i.e. ball diameter (2–4.5 mm), stirring speed (200–800 rpm) and ball charge ratio (50–80%) on the ultra–fine grinding of a refractory silver ore tailings were investigated using a pin–type vertical stirred mill.

2 MATERIAL AND METHODS

The cyanidation plant tailings of a refractory silver ore were used in the tests. Figure 1 illustrates the particle size distribution of the tailings sample (d_{80}= ≤100 μm) used in the ultra-fine grinding tests. The tailings sample consisted of 50.7% SiO_2, 9.80% BaO, 7.30% Al_2O_3, 6.76% CaO and 5.72% Fe_2O_3. The silver and gold grades were determined to be 83 g/t and 1.5 g/t, respectively. Mineralogical studies (Dinçer, 1997) have shown that silver is present mainly in the form of native silver, pyrargyrite, tetrahedrite, argentite and proustite, which are closely associated with other mineral phases i.e. mainly barite, quartz, dolomite and feldspar.

Ultra–fine grinding tests were carried out using a laboratory scale pin–type vertical stirred mill designed by the authors (Fig. 2) within a batch mode of operation. The technical features of the stirred mill were described earlier by Celep et al. (2011). Energy consumption was also monitored during the grinding period. Micro–grinding ceramic beads (alumina–based zirconia toughened, DMM AZ 2000®) in different sizes (i.e. with mean diameters of 2, 3.5 and 4.5 mm) were kindly provided by Dakot Milling Media (Pty) Ltd (South Africa) and used as the grinding media. The beads had an Al_2O_3 content of 80%, specific gravity of 3.75-3.80 g/cm^3 and vickers hardness of 1314 micro. Pulp density was kept constant at 24% w/v.

Particle size analysis was carried out by the laser diffraction method using a Malvern Mastersizer 2000 MU. Particle size analysis was performed in four replicates and the mean values were presented in the results.

Preliminary cyanidation tests confirmed the refractory characteristics of the tailings material and enhancing effect of ultra-fine grinding in the silver recovery. A 60% increase was observed with the application of ultra–fine grinding i.e. from 20% Ag recovery (d_{80}= ≤100 μm) to 80% Ag with UFG (d_{80}= ≤6.3 μm).

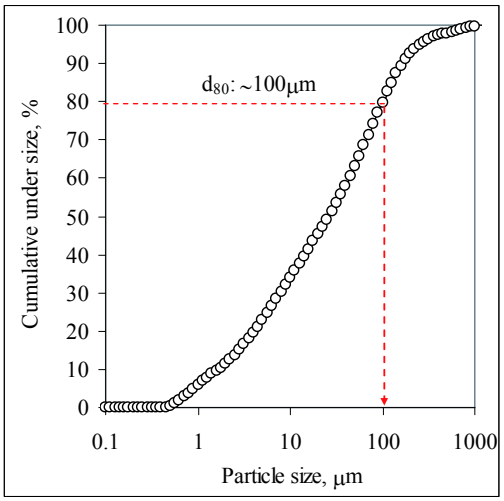

Figure 1. Particle size distribution of feed material used in grinding tests

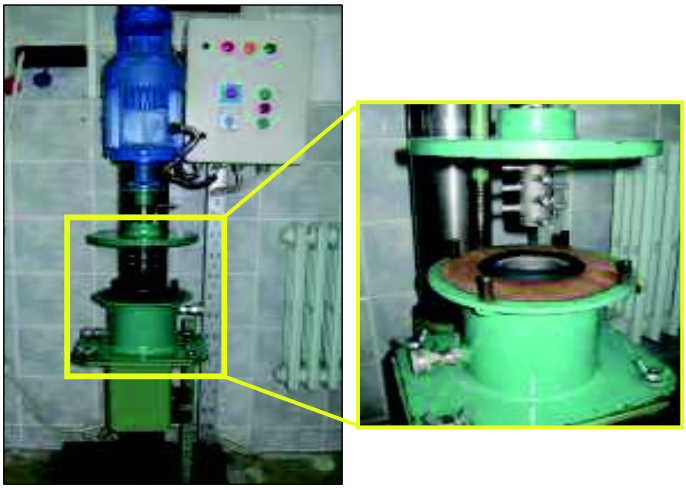

Figure 2. Section drawing of the stirred mill used in the ultrafine grinding tests

3 RESULTS AND DISCUSION

3.1 Effect of Grinding Time

The effect of grinding time (i.e. 1, 4, 8, 15 and 25 min.) on the fineness of grind (d_{80}) was investigated under the constant conditions of stirrer speeds, ball diameters and ball charge ratios (Fig 3). A significant decrease on the particle size was observed with the increase in grinding time from 1 to 15 min. Longer periods (>4 min.) were needed to achieve a d_{80} of <5 µm. It was shown that the percentage of 10 µm passing amount is increased by increasing of grinding time (Fig. 3).

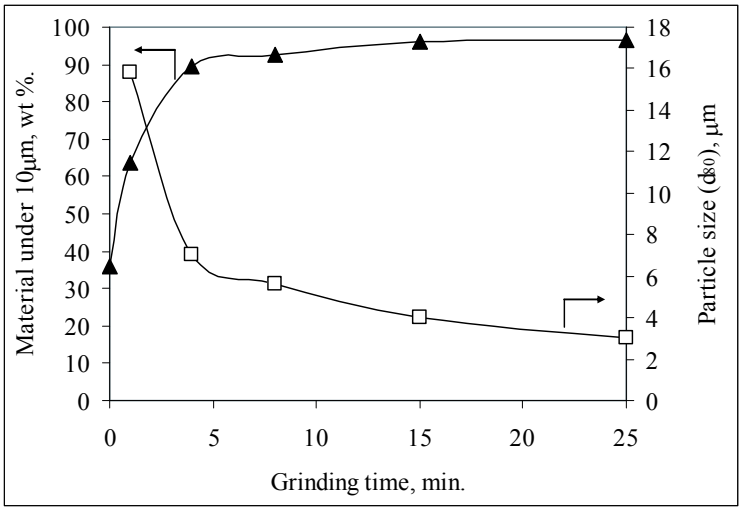

Figure 3. Effect of grinding time on particle size (d_{80}) and material amount (wt%) under 10 µm size (3.5 mm ball diameter, 800 rpm stirrer speed, 80% ball charge ratio)

3.2 Effect of Stirrer Speed

The increase in stirrer speed resulted in finer particle sizes in all grinding times (Fig 4) e.g. particle size (d_{80}) decreased from 9.7 μm to 3.6 μm with the increase in stirrer speed from 200 to 800 rpm over 15 min. Celep et al., (2011) also showed the positive effect of stirring speed. In contrast to the findings in the current study (Fig. 4) some researchers (Mankosa et al., 1989; Gao and Forssberg, 1993; Sepulveda, 1981) reported that higher speeds (i.e. up to 1350 rpm) resulted in lower energy efficiency, resulting in increase of the mean particle size. The lower energy efficiency for a higher stirring speed may be related to the fact that the energy input can not entirely be used for size reduction. In practice, an optimum stirrer speed should be selected due to occurrence of central vortex during grinding in high speeds which can limit size reduction and hence lead an increase in energy consumption dramatically (Mankosa et al., 1989; Orumwense and Forssberg, 1992).

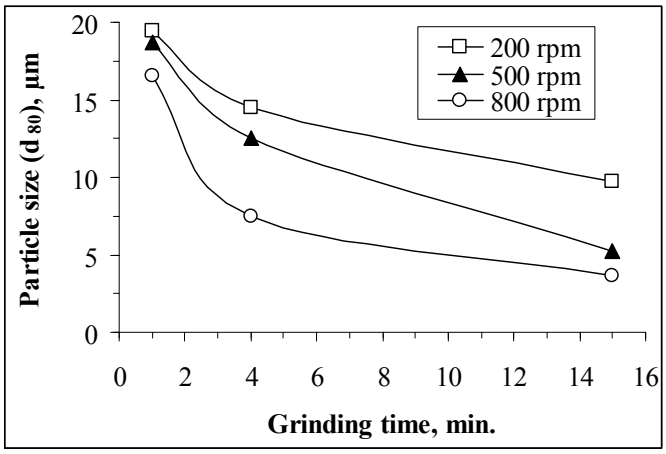

Figure 4. Effect of stirrer speeds on particle size (d_{80}) (2 mm ball diameter, 65% ball charge ratio)

3.3 Effect of Ball Diameter

Ball diameter also affects stirred milling efficiency and energy consumption (Gao and Holmes, 2007). Smaller media sizes are required to obtain finer products. Optimum ball-particle size ratio should be selected as 20:1 for maximum breakage rate (Mankosa et al., 1986) but depending on the content/quantity of minerals in the ore and type of grinding media that ratio may vary from 7:1 to 20:1 (Zheng, 1997). In the current study, ball-particle size ratios were found to be varied between 8:1 and 18:1 for all grinding tests. Figure 5 showed that coarser products were obtained by increasing the ball diameter from 2 mm to 4.5 mm.

3.4 Effect of Ball Charge Ratio

Lower particle sizes were obtained at higher ball charge ratios (Fig 6) probably due to the fact that in lower ball charge ratios grinding efficiency decreases. In stirred milling, the ball charge ratio is typically applied up to 85% which is higher than in conventional grinding systems (i.e. 40–50%) (Gao and Holmes, 2007; Celep et al., 2008). The findings (Fig. 7) also confirmed that using high ball charge ratios is necessary to achieve finer particle sizes. However, it should be noted that increasing ball charge ratio after an ideal point will have limited contribution on grinding efficiency, but can cause an increase in power draw of the mill (Gao and Holmes, 2007; Celep et al., 2011).

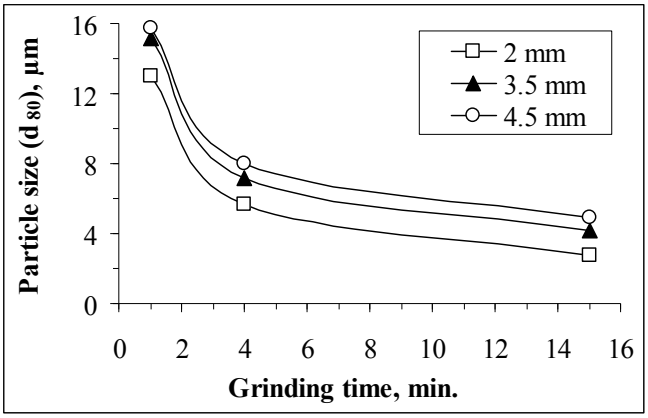

Figure 5. Effect of ball diameter on particle size (800 rpm stirrer speed, 80% ball charge ratio)

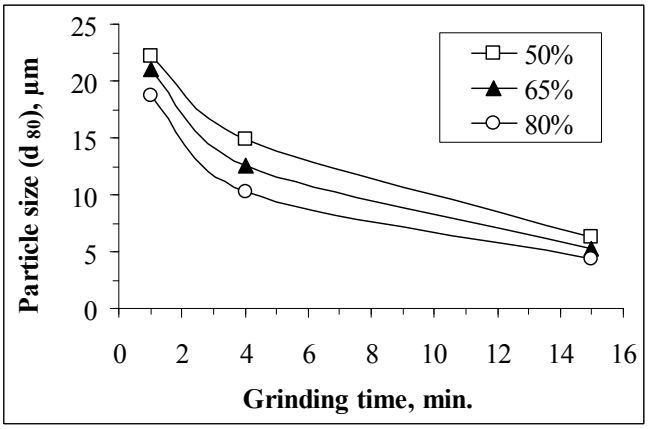

Figure 6. Effect of ball charge ratio on particle size (2 mm ball diameter, 500 rpm stirrer speed)

3.5 Energy Consumption

High energy consumptions are required to achieve a fine particle size which can be achieved by applying high stirrer speeds. At 800 rpm stirrer speed, energy consumption was increased from 62 kWh/t to 869 kWh/t to achieve finer particle sizes i.e. from 16.5 µm to 3.6 µm. Figure 7a showed that higher stirrer speeds (e.g. 800 rpm) yield the same particle size (10 µm) with lower energy consumptions (~150 kWh/t).

Ball diameter also is of importance for energy consumption. The consumed energy is increased with increasing the ball diameter related to the fact that the movement of large balls within the mill is more difficult than fine balls (Zheng vd., 1997). Same particle sizes can be obtained at smaller ball diameters by lower energy consumptions (Fig 7b). In the stirred ball mills, a large part of the energy is used to move the ball load. When increasing of ball charge ratio, the consumed energy is increased, but, the finer particle is obtained due to improve stress density within stirred mill. In the current study, the lower energy consumptions were needed to achieve same particle size when increasing of ball charge ratio from 50% to 80% (Fig. 7c).

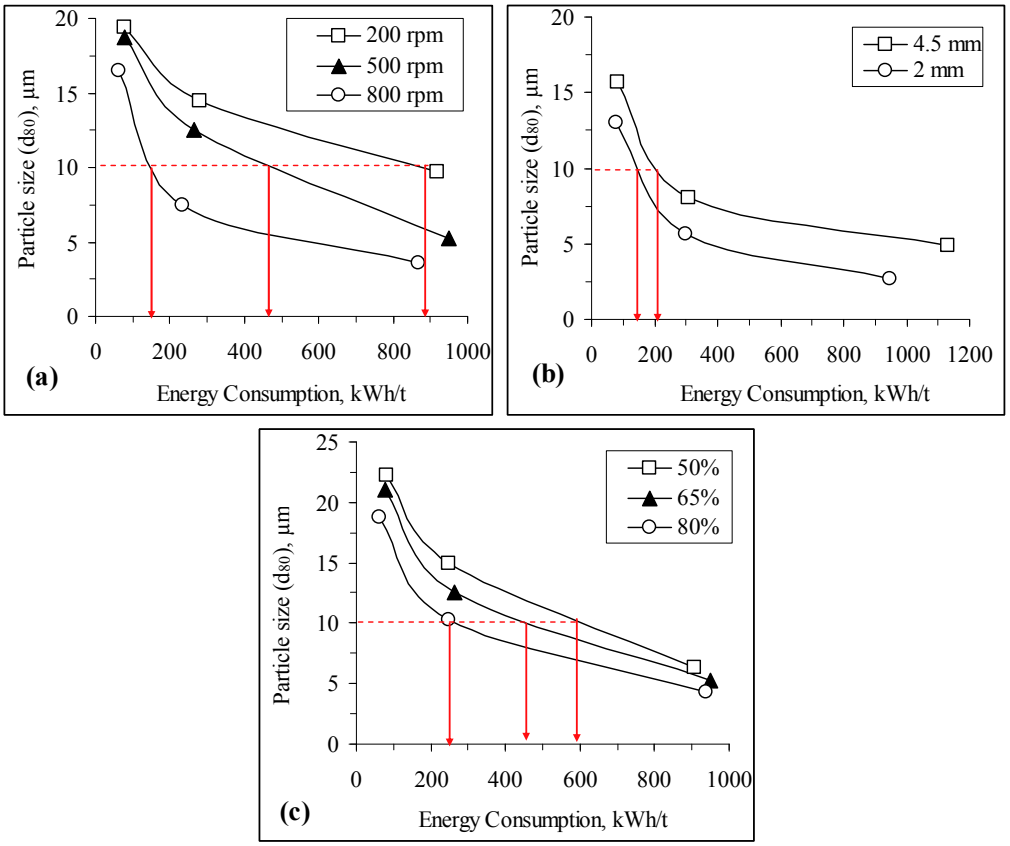

Figure 7. Relationship between particle size (d_{80}) and energy consumption a) Effect of stirrer speed (2 mm ball diameter, 65% ball charge ratio), b) ball diameter (800 rpm, 80% ball charge ratio, c) ball charge ratio (2 mm ball diameter, 500 rpm)

The operations of refractory gold/silver ores have been increasing due to exhaustion of non–refractory (free milling) ores. Pretreatment methods should be applied to refractory ores prior to the leaching stage and ultra–fine grinding as a physical method offers a viable option to conventional oxidative pretreatment methods (e.g. roasting, pressure oxidation). Commercial applications including IsaMill® and SMD® mills have been operated successfully for the treatment of such refractory ores (Davey, 2006 and 2010; Celep et al., 2010). In the current study, it was shown that, a particle size (d_{80}) of below 5 µm can be achieved over 15 min. at certain conditions of stirrer speed, ball diameter and ball charge ratio using a laboratory scale pin–type vertical stirred mill.

4 CONCLUSIONS

In this study, the effect of ball diameter (2–4.5 mm), stirring speed (200–800 rpm) and ball charge ratio (50–80%) on ultra fine grinding performance of a refractory silver ore tailings were investigated. The findings showed that at higher stirrer speeds and ball charge ratios using smaller beads finer products could be obtained. It was applicable to ground the material finer than 5 µm under suitable conditions using ceramic beads. Ultra–fine grinding process using pin–type vertical stirred mills prior to cyanidation

could be used as a physical pretreatment method to improve the cyanide leaching of silver from the refractory silver tailings.

ACKNOWLEDGEMENTS

The authors would like to express their sincere thanks and appreciation to Dr. İbrahim Alp for kindly providing the tailings sample, to Dr. Haci Deveci for proof reading the article and to Dakot Milling Media (Pty) Ltd (South Africa) for kindly providing the ceramic micro−grinding beads (DMM AZ 2000®).

REFERENCES

Celep, O., Alp, İ., Türk, T., 2008. Stirred media mills in ultrafine grinding technology and the applications in ore dressing, Review of Earth Sciences, İstanbul, 21, 2, 61-73.

Celep, O., Aslan, N., Alp, İ., Taşdemir, G., 2011. Optimization of some parameters of stirred mill for ultra–fine grinding of refractory Au/Ag ores, Powder Technology, 208, 121–127.

Ciftci, H., Akcil, A., 2010. Effect of biooxidation conditions on cyanide consumption and gold recovery from a refractory gold concentrate, Hydrometallurgy, 104, 142–149.

Corrans, I.J., Angove, J.E., 1991. Ultra fine milling for the recovery of refractory gold, Mineral Engineering, 4 (11), 763–776.

Davey, G., 2010. Ultrafine grinding applications using Metso stirred mills in precious metal processing, Proceedings of the XII International Mineral Processing Symposium, Turkey, pp.79–84.

Davey, G., 2006. Fine grinding applications using Metso Vertimill grinding mill and the Metso Stirred Media Detritor (SMD) in gold processing, 38th Annual Meeting of the Canadian Mineral Processors, Ottawa–Canada, pp. 251–261.

Dinçer, H., 1997. Benefication of Gümüşköy Silver Plant tailings and increasing the plant recovery, Ph.D. Thesis, İ.T.Ü. University, Turkey, (in Turkish).

Dunn, J.G., Chamberlain, A.C., 1997. The recovery of gold from refractory arsenopyrite concentrates by pyrolysis–oxidation, Minerals Engineering, 10 (9), 919–928.

Gao, M., Holmes, R., 2007. Developments in fine and ultrafine grinding technologies for the minerals industry, The Institute of Materials and Mining (IOM3), http://www.iom3.org.

Gao, M.W., Forssberg, E., 1993. A study on the effect of parameters in stirred ball milling, International Journal of Mineral Processing, 37, 45–59.

Gunyanga, F.P., Mahlangu, T., Roman, R.J., Mungoshi, J., Mbeve, K., 1999. An acidic pressure oxidation pre–treatment of refractory gold concentrates from the Kwekwe roasting plant–Zimbabwe, Minerals Engineering, 12 (8), 863–875.

Jankovic, A., 2003. Variables affecting the fine grinding of minerals using stirred mills, Minerals Engineering, 16, 337–345.

Jankovic, A., Valery, W., 2004. Fine and ultra fine grinding–the facts and myths, The 6th Annual I.I.R. Crushing and Grinding Conference. Perth, Australia.

Kwade, A., 1999. Wet comminution in stirred media mills–research and its practical application, Powder Technology, 105, 14–20.

La Brooy, S.R., Linge, H.G., Walker, G.S., 1994. Review of gold extraction from ores, Minerals Engineering, 7 (10), 1213–1241.

Lichter, J., Davey, G., 2006. Selection and sizing of ultrafine and stirred grinding mills, In: Advances in Comminution, S. Kawatra (Eds.), Society for Mining, Metallurgy and Exploration, Inc., Colorado.

Mankosa, M.J., Adel, G.T., Yoon, R.H., 1986. Effect of media size in stirred ball mill grinding of coal, Powder Technology, 49, 75–82.

Mankosa, M.J., Adel, G.T., Yoon, R.H., 1989. Effect of operating parameters in stirred ball mill grinding of coal, Powder Technology, 59, 255–260.

Marsden J. O., House C. I., 2006. The chemistry of gold extraction, Society for Mining, Metallurgy, and Exploration, Inc. (SME), Littleton, USA.

Orumwense, O.A., Forssberg, E., 1992. Superfine and ultrafine grinding–a literature survey, Mineral Processing and Extractive Metallurgy Review, 11, 107–127.

Sepulveda, J.L., 1981. A detailed study on stirred ball mill grinding, Ph.D. Thesis, University of Utah, USA.

Tüzün, M.A., Loveday, B.K., Hinde, A.L., 1995. Effect of pin tip velocity, ball density and ball size on grinding kinetics in a stirred ball mill, International Journal of Mineral Processing, 43, 179–191.

Zheng, J., 1997. Stirred media mills: dynamics, performance and physico–chemical aspects, Ph.D. Thesis, Colombia University, USA.

Kırma Tesis Operasyonlarının Performansını Etkileyen Faktörler
Factors Affecting the Performance of Crushing Plant Operations

E. Yılmaz
Inmet Mining Corporation, Toronto (Ontario) Canada
Çayeli Bakır İşletmeleri A.Ş., Madenli Beldesi, Çayeli (Rize), Turkey

ÖZET Proses operasyonları sürdürülebilir ilerlemeyi dikkate almayı gerektirdiğinden kırma tesislerine cevherlerin partikül boyutunu azaltmada büyük ilgi olmuştur. Kırma tesisleri zor koşullarda opere edildiği ve çok abrasif malzemeye maruz kaldığından dolayı çeşitli faktörler onların performansını etkileyebilir. Bu bildiri kritik tasarım parametrelerinin yanında cevher özellikleri, işlerlik ve sürdürülebilirliği hesaba alarak Çayeli madeni kırma tesis operasyonun performansına etkileyen faktörleri sunmaktadır. Bildiri ayrıca kırma tesisinin operasyonel, enstrümental, mekaniksel ve bakım yönlerini ele alan raporlama sistemini de sağlamaktadır. Birincil sonuçlar hali hazırda madende uygulanan bu yeni sistemin iyi bir şekilde çalıştığını ve mevcut kırma tesisi yönetimine yeni bir perspektif getirdiğini göstermektedir.

ABSTRACT Crushing plants have been of great interest in reducing the particle size of ores milling operations need to consider sustainable development. Since the crushing plants are operated under severe conditions and subjected to very abrasive material, several factors can influence their performance. This paper presents factors affecting the overall performance of the Çayeli mine crushing plant operation by addressing the critical design parameters as well as the consideration of ore characteristics, operability and maintainability. It also provides a reporting system, which considers the operational, instrumental, mechanical and maintenance aspects of crushing plant. Preliminary results show that this new system being implemented at mine is running well and brings a new perspective to the present crushing management.

1 INTRODUCTION

In the industries supporting the mining and milling operations, crushing plays a massive role in reducing the particle size of rocks and ores. To reach desirable end product size, the feed material endures a few crushing stages that form a circuit. A crushing plant system consists of a combination of unit operations for storing, feeding, crushing, screening, and conveying (Viilo, 2011). Crushing plants are often designed to be able to produce certain throughput on predefined specification and the size distribution while keeping the plant capacity and quality, resulting a reasonable cost and energy consumption (Beerkircher et al., 2003, Lindqvist, 2008; Asbjörnsson et al., 2012). The main challenging of running a crushing plant as competently as possible knows how each production unit affects the efficiency of the whole plant (Svedensten and Evertsson, 2004). Therefore, these units should be built up with the technologies and improvements which give savings at great amounts for every ton of ore crushed, a high capacity of use, the ability to consume little energy, and low repair-service costs (Utley, 2003; Wills and Napier-Munn, 2006).

Crushing plants like any other production process are greatly affected by changes over time since it is a continuous process where equipment is subjected to variations. These variations can be caused by unmatched or degrading equipment performance which can be minimized overall plant capacity and thus the decreased product quality (Major, 2003; Bengtsson et al, 2009; Itavuo, 2009). In order to attain a certain product quality, numerous crusher settings (i.e., closed size setting CSS, speed, etc) can be varied by plant operators on a daily basis. Ore properties play also a vital role on the quality of product and plant performance (Schönert, 1996; Guimaraes et al., 2007). Practitioners are striving to build up better and more reliable crushing plants. One of the central functions of well-running and professionally-managed crushing plants is to present several documents for owners, engineers, operators, practitioners, or even visitors (Boyd, 2008). Those documents will allow them to review and better understand recent developments in operating areas.

In this paper, factors that affect the overall performance of the crushing plant operations at the Çayeli Mine are evaluated by focusing several critical design parameters associated with downtimes and production losses. As well, it provides a crusher reporting system, developed a macro in MS Excel, which deals with operational, instrumental, mechanical and maintenance aspects of crushing plant. It is hoped that the paper will provide a basic knowledge on how crushing is conducted at the mine without causing any significant loss of the variables monitoring the safety and environmental subjects while maintaining its operations in a sustainable aspect. Specific objectives are: *i)* to get detailed knowledge which can be used for assessing the crushing plant performance and control development, *ii)* to collect a bunch of system data which can be used for calculating plant availability and utilization, and *iii)* to better describe the bottlenecks of crushing plant which can lead to production delays.

2 ORE CRUSHING PLANT

The Çayeli mine is the first fully mechanized underground copper and zinc mine operating since 1994, located in the province of Rize, Turkey. The mine is owned and operated by Inmet Mining Corp. (Toronto, Canada).

Run of mine ore is delivered directly from both the underground and over a distance of 1 km from the shaft to the stockpile (having a 24,000 t capacity) by trucks. Based on their types and grades, the ores hauled are then stored to bins. To get optimal metallurgical results, the ore is blended and fed to crusher by loader bucket for size reduction. Crushing is done in three stages with a grouping of a jaw crusher and two cone crushers that work in close circuit with screen (Figure 1).

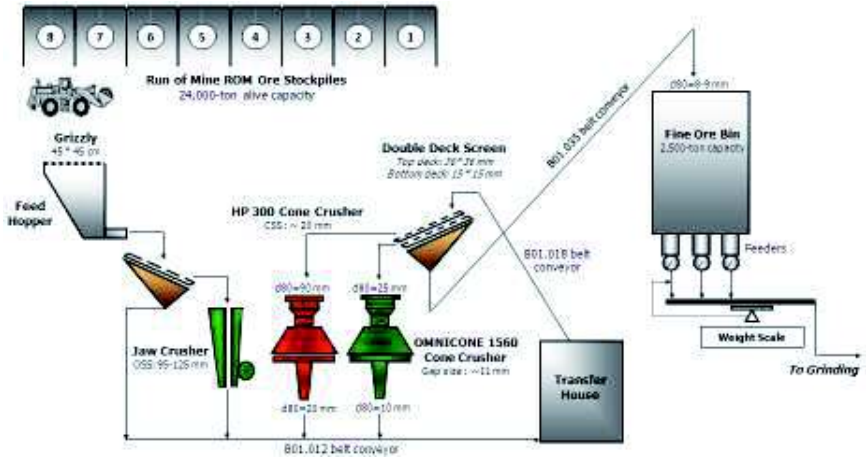

Figure 1. A typical flow sheet for the Çayeli crushing plant operations

Feed hopper which feeds jaw crusher has 50-t capacity and it has a 45×45 cm grizzly screen on it. The materials, finer than 45 cm, pass through screen. At entry of jaw crusher, there exists a vibrating feeder equipped with steel chains for homogeneous feeding. 80% of crusher final product is minus 8-9 mm. A rock breaker is also used to break oversize rocks accumulating over feed hopper grizzly. Crushing circuit consists mainly of jaw and cone crusher, double deck vibrating screens, belt conveyors, transfer house, fine ore bin, metal collection systems (magnets and metal detectors), and de-dusting system.

3 FACTORS AFFECTING CRUSHER PERFORMANCE

There are a number of factors that can affect the production performance in ore crushing plant (Figure 2). However, these factors can be illustrated under the three most important categories of influence: ore characteristics; equipment factor, and operation factor. The aspects affecting the process are site-specific and subjected to change based on operation. Identifying problems and debottlenecking in a crushing plant is a challenging task since it requires info and experience of the plant. The bottleneck in an open circuit is often the last production unit which ensures steady output from plant. In closed circuit, it may however a bit more complex, causing problems.

3.1 Ore Characteristics Factor

Material characteristics play a major role on the quality of the end product in the crushing plant. The ore entering the crusher will affect the plant performance, based on its change in mineral content, grain size distribution, and moisture. In addition, the ores that contain non-ore products, such as sticky, mixed-up, wet, and dry materials, metals, woods, and plastics can possess an influence on crusher performance, resulting in lower production rate. Wet, sticky ores may clog chutes, lessen the live storage capacity of bins or silo. Drier ores are generally dustier because they are likely to stick together into larger particles.

Based on their mineralogical composition, copper and zinc grades, there exist six types of run-of-mine ore: yellow ore YO, black ore BO, clastic ore CO, bornite yellow ore BYO, bornite clastic ore BCO and low grade ore LYO. CO contains more than 10% sphalerite clasts in matrix. BO and YO types are based on contained zinc grade and mined singly to allow for the most favourable grade blending from the bins. These ore types are referred to as “Spec Ore”. BO is defined as the ore with more than 4.5% Zn and a Cu/Zn ratio of less than 1. YO consists typically of pyrite and chalcopyrite clasts, up to 20 cm in size, in matrix containing less than 10% sphalerite.

Figure 3 shows fine sections of different ore types: BO, CO, YO, LYO, BCO, and BYO. Although CO looks like a hard ore in its physical appearance initially, its crushing process is easy due to many small scattering grains. These grains are very susceptible to breaking because they are the residues of weathering. One can also say that bornite could exhibit the plastic behaviour in which crushing may become problematic. However, bornite-free ores such as YO, BO, and LGO act as massive sulphide blocks, and can be crushed in a hardly manner. The loose joints and well-developed ores, such as CO are easily broken in the crushing plant.

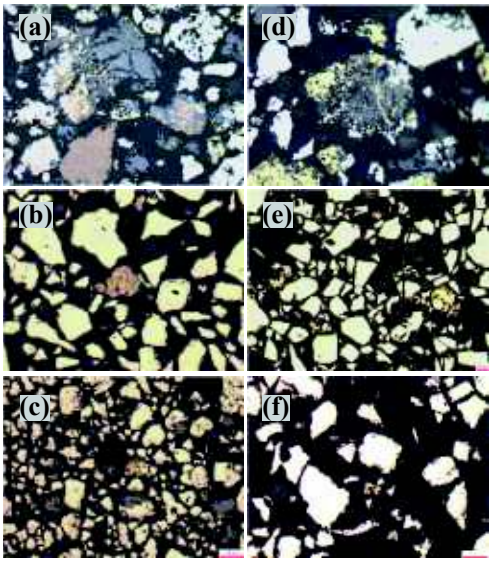

Figure 3. Fine sections of ore types: a) BCO; b) BYO; c) BO; d) CO; e) YO; and f) LYO

Figure 2. Cause-and-effect diagram over factors affecting plant performance

Figure 4 shows the variation in the total amount of ore crushed for the year 2012. It can be easily witnessed that crusher put up in a fairly good performance this year, except for April, in which the production remained behind a threshold value of 100,000 wmt, resulting in a production rate of 94,610 wmt The cogent reasons behind this phenomenon is the mechanical/instrumental, maintenance and operational downtimes, causing a drop in the production for a time period of 66, 57, and 110 hours, respectively.

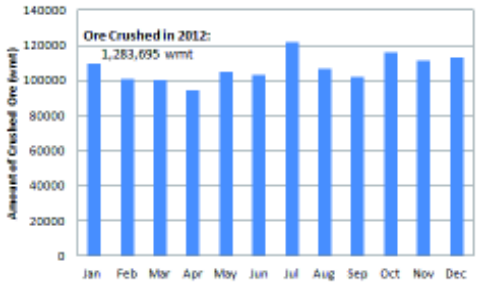

Figure 4. Change in ore crushed in the plant

The important factor is that if stockpiling run-of-mine ores are clean, excluding non-ore materials, such as wood, plastic, metal, etc, and their brittleness indexes are high, the ore is being crushed in a quicker and easier way without causing problem. More fragile particles are effortlessly broken into smaller particles. The harder the ore is, the higher compressive strength is and more easy to be crushed. The capacity of crusher will be low strictly if the ore contains more chunks, dust, wet, and ore fines which will finally expand the stickiness of ore and accordingly reduce ore discharge speed.

As discussed in earlier sections, there are six different ore types in order to make four campaigns as follows: Spec, Non-spec CO, BCO and BYO. Table 1 lists the crushed ore according to campaign type and distribution. The use rates of Spec, CO, BYO, and BCO campaigns are respectively 29%, 42%, 10%, and 19%, taking into consideration a crusher throughput of 1,283,695 wmt. The most problematic ore campaign is BCO since its mineralogy (i.e., bornite) shows differences to the others (Figure 3). They take steps in a different way during crushing: Some of them will be crushed readily while others generate difficultness to be crushed efficiently. The degree of difficultness will vary according to the texture of bornite-bearing minerals.

Table 1. Distribution of types of ore crushed according to ore campaigns

Blend Type	Crushed Ore (%)	Ore Type Distribution (%)					
		BO	YO	CO	LGO	BYO	BCO
Spec	29	14	59	13	10	3	0
CO	42	6	1	74	8	1	11
BYO	10	1	5	2	6	82	3
BCO	19	5	0	12	9	6	68

Experiences indicate that the best crushing performance is respectively obtained from CO, YO, BYO, and BCO campaigns. Due to the fact that CO contains hordes of broken fragments within ore mass in micron size, its breakable rate is higher when compared with the others. In fact, these fragments disperse homogenously in the ore and help to increase crushing performance of the ore.

Figure 5 shows the variation in crushed ore in a month, taking into consideration six different ore types. The results reveal that the usage percentages of CO, BCO, YO, BYO,

BO, LGO are respectively 36, 19, 18, 11, 8 and 8%. Bear in mind that the usage amounts of the ores by month are strictly depending on both the present ROM ore availability at stockpile area and the campaign switches.

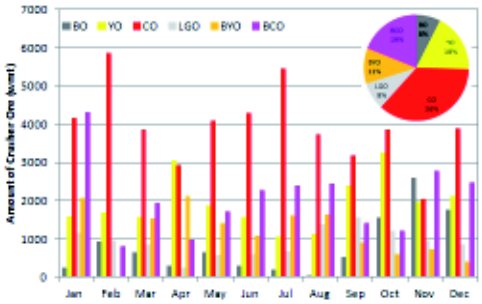

Figure 5. Distribution of ore crushed, taking into account ore types

Overall, a specific order for ore campaigns is used as following: Spec → BYO → Non-Spec CO → BCO → BYO → Spec. Because of the high availability of clastic ore being extracted from underground; this type of ore is most often used in the crushing plant for Spec (with YO) and Non-Spec (with BO) campaigns. Low grade ore LGO is hauled from underground as least as possible since overall stockpile copper and zinc grades are decreased appreciably.

3.2 Equipment Factor

To control the quality of ore produced from a crushing plant, the appropriate equipments should be selected for sustainable operation. The choice of crusher equipments depends on the type and amount of material to be crushed. The equipment parameters, such as speed, model, and less maintenance need are closely related to the success of a confident level of product quality. The higher rotate speed can increase crusher productivity, but consume more energy, and may go ahead to blockages. Due to the fact that changing the equipment parameters affects the product quality, they are more susceptible to changes at any time, based on the crusher production requirements.

Figure 6 shows the usage hours of three loaders and rock breaker, which are the key items to feed the ore stockpiling to crusher. It is clear that the usage of 17-662 loader is reduced while increasing the usage of 17-655 and 17-663 loaders over time. Note that 17-663 loader is used as spare loader as others are out of service. Rock breaker shows a stable usage over the years since it is often used for crushing the coarse-size ores on feed hopper grizzly in the beginning and end of shifts. It is also good to mention that loaders are crucial to crushing and milling operations since blending and concentrate loading are made with them.

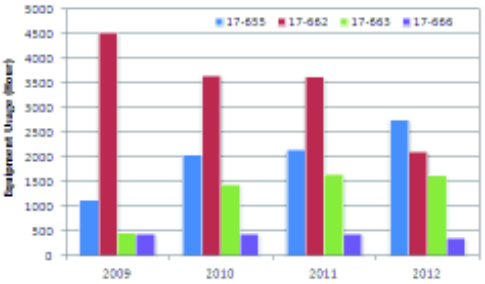

Figure 6. Usage hours of three loaders and rock breaker used in crushing operations

Figure 7a shows the change rapidity and costs of bottom deck vibroflex, polyurethane screens (800×1850 mm). The bottom deck screens (15×15 mm) are constantly subjected abrasive wear due to ore's relative motion. To prevent overloading in circuit and reduce the wear rate of screen, vibroflex screens which are anti-static and hydrophobic are preferred. Initially, screen apertures were often being plugged and tried to open them by using air pressure. The change rate of bottom decks is increased from a time period of 30-45 days, based on a well collaboration between mechanical and operational teams. Figure 7b shows the change frequency and costs of top rubber-clad screens (600×300 mm). Since its aperture is 36×36 mm that enabling larger ore rocks feeding to tertiary crusher, the wear of screens remains low and so their change frequency happens in the range of six months to one year.

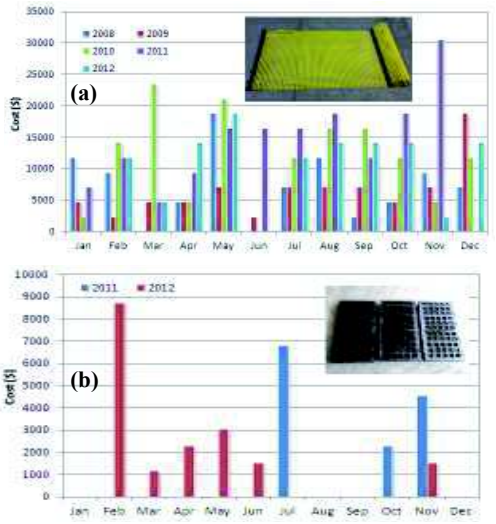

Figure 7. The cost change in bottom (a) and top deck (b) screens as a function of time

Figure 8 shows the change frequency and connected costs of the major equipment used in the crushing plant, which include crusher, feeder, screen, conveyor, air cannon, magnet, and metal detector. The cost change is taken into account as a function of time.

Crushing performance is directly based on the operating time of the equipment without being out of service. Change in performance due to wear differs acutely depending on the feed material and equipment. Wear plates are of great importance in lasting the lifetime of the liners and crushers and therefore high manganese plates are utilised by increasing the capacity and obliging less mechanical repair. On the whole, the maintenance costs of both jaw and cone crushers are decreased palpably in 2012. The key reason behind this reduction may be well explained by oil and lubrication systems, and by reduced crusher wear parts. A serious improvement in feeder, chutes, and conveyor are realized by keeping the particle size distribution of the crushed material. However, the cost for B01.012 belt conveyor seems to be increased lately. This is mainly due to a number of sharp metals or objects which are directly dropped on the conveyor by causing the brutal damages. To prevent this happening again, a rip detection system is installed in this belt conveyor.

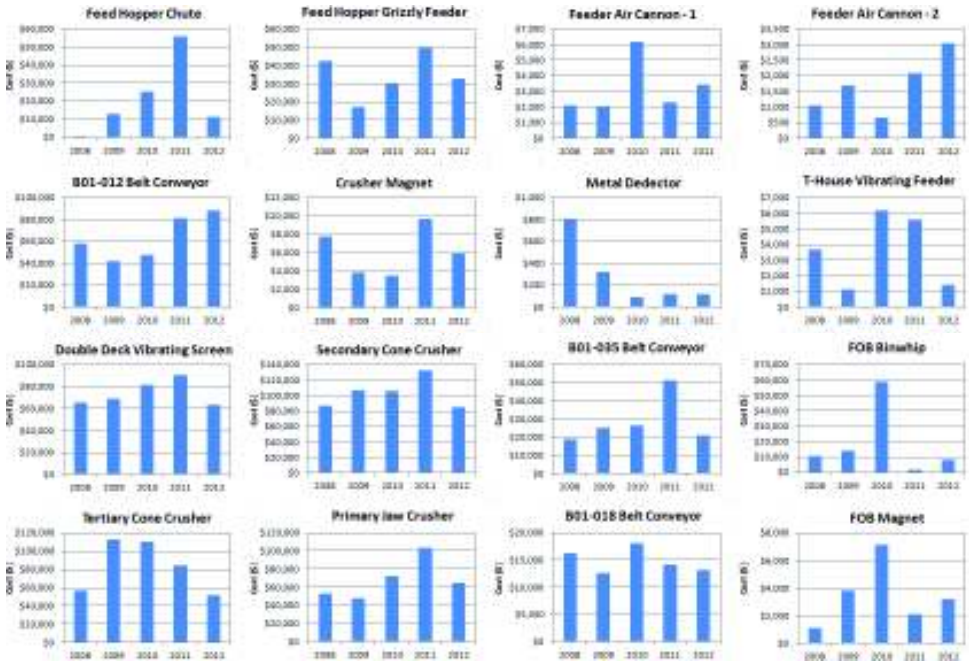

Figure 8. The cost change in the major equipment of the crushing plant

In addition, the double deck screen costs are significantly reduced by implementing a new strategy during and after its placement. Strategy is relied on the more maintenance and care for a couple of days just after panel replacement, and also the clean-up process of non-ore materials (i.e. plastics and woods) on screens at shift breaks on a daily basis. Due to a more efficient blend preparation, magnet and metal detector costs are also lowered to a great extent while air cannon costs are dimly increased recently. This increase is due to wet, sticky ores which may clog the surfaces of air cannon and therefore deteriorates their functions properly. This situation is observed especially in the winter season.

3.3 Operation Factor

An efficient operation of rock crusher plays an important role on crushing productivity. Not only the design and layout of equipment, but also the cost of running them should be considered to reach the best performance of plant. This is succeeded by operators and their practical appliances during shifts. To meet production goals for a given budget, the equipment used for crushing should have high operating availability, which is achieved by keeping maintenance requirements to a minimum level as much as possible.

Figure 9 illustrates the change in crusher performance in terms of both availability and utilization percents. The average availability and utilization rates were respectively 89% and 78%, thus corresponding to an overall asset utilization of 69%. Note that February 2012 conferred the best performance.

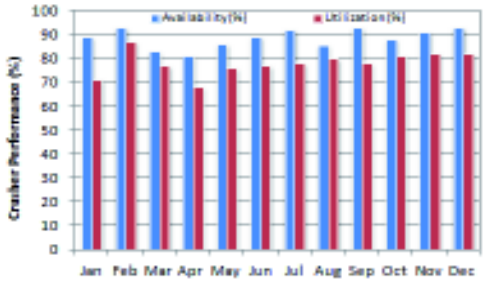

Figure 9. Change in crusher performance in terms of availability and utilization

There are also several production losses at crushing plant which can cause a disruption in normal operations leading to inefficiency, and thereby increase costs. Figure 10 shows the change in production losses which are mainly categorized as ore, selection of non-ore material retained over the conveyor, rock breaker, and fullness induced by wet, sticky ores. One can conclude that during the winter season, ore may become problematic due to raining and inadequate ore production. This causes to fullness of cone crushers, secreens and t-house. Producton loss induced by rom ore, selection, rock breaker and fullness were respectively 259, 887, 273, and 611 minutes.

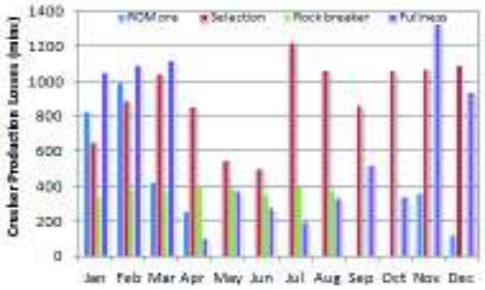

Figure 10. Change in crusher production losses as a function of ore, selection, rock breaker, and fullness

To boost the crushing plant performance, a project relating to non-ore material sorting from the ROM ores stockpiled just before let them introduce to plant is in progress. There existed sometimes in crushing plant in which the system is non-operational, and keeps downtime associated with mechanical repair, corrective and preventive maintenance work, instrumental and operational delays. Figure 11 shows the change in crusher down times. It is shown that the down times induced by maintenance, operational, mechanical, and instrumental were 2862, 5049, 2015, and 328 minutes. The most down times are caused by operational issues as follows: daily clean-up, chute plugs, crusher plugs and settings (close side setting which enables the production of products in desirable size). Operators have to regularly clean cone crusher and bottom deck screen chutes for 30 minutes during shift.

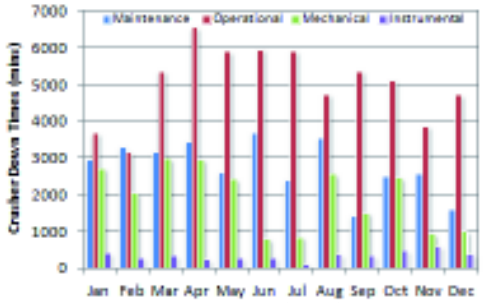

Figure 11. Change in crusher down times as a function of maintenance, operational, mechanical and instrumental

Attention must be paid that operators need to check a number of equipment set-ups if their functions are running well. In fact, there has to be a clearance distance of 90 mm between fixed and moving jaws for jaw-type crushers. This clearance distance gets larger when wear appears on the jaws. Shims are mounted to the studs which are holding the jaws to lessen the clearance to 90 mm, when it reaches to more than 120 mm. As mantle wears, the bowl is also tightened in order to increase the pressure on mantle. The aim is to take mantle closer to bowl since crushing action is accomplished between mantle and bowl. This is also known as adding bar.

Figure 12 illustrates the change in metal alarms, which are considered as one of down times experienced at crushing plant. Data is presented monthly as both count and time. Considering that each metal alarm takes five minutes, the average count and time of metal alarms were respectively 520 and 43 hours.

Figure 12. Change in metal alarms as a function of count and time

The total number of the metal-induced alarms are corresponded to 22 days, which stop running the plant. To end up the number of metal alarms, a project is initiated recently to sort the metals within ores stockpiled in bins. Preliminary results prove that crusher performance is getting superior.

One of the contributions behind the metal sorting at stockpile is also that the number of damages to both belt conveyors and crushers, causing belt cuts and crusher blockages is dropped significantly. This also makes these items to remain in operation, which increases their availability and utilization rates.

Figure 13. Photos showing cone crusher and double deck screen plugs

The non-ore material selection project will also help decrease both crusher and screen plugs, as shown clearly in Figure 13. Due to the fact that the ores entering the circuit is metal-, plastic-, and wood-free, the apertures of screens, and the chutes will never block. This project is hoped to reduce circulating load, maximize profit and desirable fractions, and increase the crusher throughput.

4 CONCLUSIONS

This paper summarizes factors that affect the performance of Çayeli Mine crushing plant operations. There are three foremost factors of influence: ore characteristics, equipment and operation. Besides the other factors, the operation factor can contribute positively to the performance if well managed. However, due to the fact that ore properties will remain

the same during processing, its control may be tricky for product quality. In controlling the crushing plant performance, operator must consider these three factors in unison since one may change strictly the quality of the end product to a great extent while the others have a lesser effect on product.

Based on the results of the present study, the following conclusions can be drawn:

- Crusher settings play a leading role in achieving the product quality. Regular controls can augment the performance of crushing plant operations.
- The optimal ore blending will decrease appreciably the need of corrective and preventive maintenance, thus reaching higher operating availability.
- Sorting the non-ore material within the ores which will travel over the plant is of great importance in increasing the crushing performance and should keep continuing for enhanced operations.

This paper has shown that a newly-started reporting data for crushing plant will bring a new outlook in assessing the performance of production units in terms of availability and utilization rates. As well, it will come out the crushing plant's failing directions and ensure a quick solution in a timely manner.

ACKNOWLEDGEMENT

The author would like to express his profound gratitude and sincere appreciation to the senior management of the Çayeli Bakır İşletmeleri A.S. for granting permission and helpful support to publish this conference paper. Mill management, including engineers, supervisors, and operators, who directly or indirectly contribute to this work are gratefully acknowledged. Special thanks are also due to S. Yılancı for mineralogical testing, G. Çalışkan for reporting remarks, S. Sarvan for mechanical information, N. Bilgin for geological notices, and S. Arıcı for data processing.

REFERENCES

Asbjörnsson, G., Hulthén, E., Evertsson, M., 2012. Modelling and dynamic simulation of gradual performance deterioration of a crushing circuit – Including time dependence and wear, *Minerals Engineering,* Vol. 33, pp. 13-19.

Beerkircher, G., O'Bryan, K., Lim, K., 2003. Selection and sizing of secondary and tertiary cone crushers, *Mineral Processing Plant Design, Practice, and Control – Vol. 2,* (eds: A.L. Mular, D.J. Barratt, D. N. Halbe), SME, pp. 621-627.

Bengtsson, M., Svedensten, P., Evertsson, M., 2009. Improving yield and shape in a crushing plant, *Minerals Engineering,* Vol. 22, pp. 618-624.

Boyd, K., 2003. Crushing plant design and layout considerations, *Mineral Processing Plant Design, Practice, and Control – Vol. 2,* (eds: A.L. Mular, D.J. Barratt, D. N. Halbe), SME, pp. 669-697.

Guimaraes, M.S., Valdes, J.R., Palomino, A.M., Santamarina, J.C., 2007. Aggregate production: fines generation during crushing, *International Journal of Mineral Processing,* Vol. 81, No. 15, pp. 237-247.

Itavuo, P., 2009. Dynamic modelling of a rock process, *M.Sc. Thesis,* Tampere University of Technology, Finland, pp 1-112.

Lindqvist, M., 2008. Energy considerations in compressive and impact crushing of rock, *Minerals Engineering,* Vol. 21, No. 9, pp. 631-641.

Major, K., 2003. Types and characteristics of crushing equipment and circuit flowsheets, *Mineral Processing Plant Design, Practice, and Control – Vol. 2,* (eds: A.L. Mular, D.J. Barratt, D. N. Halbe), SME, pp. 566-583.

Schönert, K., 1996. The influence of particle bed configurations and confinements on particle breakage, *International Journal of Mineral Processing*, Vol. 44-45, No. 3, pp. 1-16.

Svedensten, P., Evertsson, M., 2004. Crushing plant optimisation via a genetic evolutionary algorithm, *Minerals Engineering,* Vol. 18, pp. 473-479.

Utley, R.W., 2003. Selection and sizing of primary crushers, *Mineral Processing Plant Design, Practice, and Control – Vol. 2,* (eds: A.L. Mular, D.J. Barratt, D. N. Halbe), SME, pp. 584-605.

Viilo, K., 2011. *Crushing and Screening Handbook,* 5th ed., Metso Minerals, Tampere, Finland.

Wills, B.A., Napier-Munn, T., 2006. *Wills' Mineral Processing Technology (7th ed.)-An Introduction to the Practical Aspects of Ore Treatment and Mineral Recovery,* Burlington, United States, Butterworth-Heinemann (Elsevier).